ELSEVIER

Journal of Non-Crystalline Solids 262 (2000) 35–65

JOURNAL OF NON-CRYSTALLINE SOLIDS

www.elsevier.com/locate/jnoncrysol

Magnetic resonance studies on radiation-induced point defects in mixed oxide glasses. II. Spin centers in alkali silicate glasses ☆

Ilya A. Shkrob *, Boris M. Tadjikov, Alexander D. Trifunac

Chemistry Division, Argonne National Laboratory, 9700 South Cass Avenue, Argonne, IL 60439, USA

Received 16 April 1999; received in revised form 8 October 1999

Abstract

Irradiation of alkali silicate glasses results in the formation of metastable spin centers, such as oxygen hole centers (OHC_1 and OHC_2), silicon peroxy radicals and a silicon dangling bond (E′ center). In this work, electron paramagnetic resonance (EPR) and electron nuclear double magnetic resonance (ENDOR) are used to study these spin-1/2 defects. It is shown that in a subset of the OHC_1 centers the $\equiv SiO\cdot$ radical is strongly coupled to a single alkali cation. Thermally activated swinging motion of this cation causes asymmetric T_2 relaxation and changes electron spin echo envelop modulation (ESEEM) spectra. It is argued that trapping of the hole by non-bridging oxygen atoms does not result in the release of a compensating alkali cation. Rather, the O–Alk bond elongates and the whole structure relaxes. This view is supported by semi-empirical and ab initio calculations. The observed axial symmetry of the *g*-tensor for OHC_2 is the result of rapid tunneling of the electron between two degenerate sites with rate $(0.2-50)\times 10^{11}$ s^{-1} and activation energy ~10 meV. This center is a hole trapped on a tetrahedral $>SiO_2^{2-}$ unit or a planar $-SiO_2^-$ unit. It is demonstrated that silicon peroxy radicals are not formed by charge trapping. Their generation is temperature-independent and occurs via the decay of self-trapped excitons. It seems likely that the same process yields silicon dangling bond centers.

PACS: 61.82.Ms; 71.23.Cq; 76.30.Mi; 76.70.Dx

1. Introduction

This paper continues a series of works on radiation-induced point defects in mixed oxide glasses (the studies on alkali borate glasses were reported in part I [1]). In this paper, we examine new results on magnetic resonance of O- and Si-centered radicals in vitreous alkali silicates.

Our study is brought out by a concern about radiation damage in borosilicate glass forms used for storage of radioactive waste, in particular, growth of O_2 bubbles in such glasses [2–4]. This

* Corresponding author. Tel.: +1-630 252 9516; fax: +1-630 252 4993.

E-mail address: shkrob@anlchm.chm.anl.gov (I.A. Shkrob).

0022-3093/00/$ - see front matter
PII: S0022-3093(99)00669-9

process was observed in most of silicate and borosilicate glasses, including simulated waste forms [3,4], but not in pure fused silica [5–7]. Though the yield of interstitial O_2 is low, ca. $1 \times 10^{-6} - 5 \times 10^{-6}$ molecules per eV [5–7], at the total dose of 10^9 Gy the concentration of radiolytic O_2 exceeds the solubility threshold, and the gas coalesces into 0.01–1 μm bubbles [3,4]. Given that the total dose accumulated by the glass in the first 10 kyr can be $>10^{10}$ Gy [2], up to several wt% of the matrix may disintegrate during the storage. To assess and mitigate this damage, the mechanism for formation and agglomeration of O_2 and oxygen-related defects must be determined.

We preface the discussion with a brief review of structural properties and radiation chemistry of alkali silicate glasses. The absence of such a review in the literature is one of the reasons for slow progress in understanding the radiation damage in these glasses. We include only the data that set the background for our EPR study.

Electron paramagnetic resonance (EPR) studies on spin centers in silicate glasses are more challenging than in borate glasses [1], since magnetic isotopes of silicon (^{29}Si, spin-1/2) and oxygen (^{17}O, spin-5/2) have low natural abundance (4.7% and 0.04%, respectively). Thus, costly isotope substitution is needed to find the arrangement of network-forming silicon and oxygen atoms. Fortunately, naturally occurring isotopes of alkali nuclei are magnetic (with spin-3/2 for ^{7}Li, ^{39}K, ^{23}Na and spin-7/2 for ^{133}Cs) and their spatial arrangement can be studied with several magnetic resonance techniques, including electron spin echo envelope modulation (ESEEM) [8] and electron nuclear double resonance (ENDOR) [9]. Though this information is insufficient to determine the complete structure of the spin defects (the arrangement of Si and O atoms is still unknown), it helps to choose between the available models. Further refinement of these models requires magnetic resonance studies on isotope-substituted glasses.

2. Background

2.1. The structure

The structure of alkali silicate glasses is best represented as a random network of corner-joined SiO_4 tetrahedrons whose non-bridging oxygens are compensated by alkali cations (Alk^+) [10]. Since these glasses are quenched melts, the spatial distribution of alkali cations and the speciation of SiO_4 tetrahedra reflect chemical equilibria set in the melt. On the microscopic scale (0.1–5 nm), the distributions of Alk^+ around bridging oxygens (BO) and non-bridging oxygens (NBO), as well as the Alk–Alk distribution, are non-random [10–21]. The increasingly popular view of the glass microstructure is a 'modified random network' model [10,11] in which the alkali cations line microscopic tunnels inside the network of SiO_4 tetrahedra. Recent data on ^{29}Si NMR [22–25], X-ray and neutron diffraction [10,11], XPS, EXAFS and XANES [11,12] and molecular dynamics (MD) computations [14–21] give a consistent picture of the glass structure: K^+ and Na^+ cations are coordinated with 5–6 oxygens, of which at least one oxygen is non-bridging and the rest are bridging. For Li^+, the coordination number is ~4, for Rb^+ and Cs^+, it is ~7–8. The oxygen cage is tightly fit to the cation; even the cation of smaller diameter cannot be trapped inside the cage without considerable reorganization (this results in the so-called mixed alkali effect [26–30]). The NBOs tend to cluster in the melt which in turn causes clustering of alkali cations in glass. Even for relatively low alkali loading, a substantial fraction of silicon atoms has less than three BOs: for example, in $Na_2O \cdot 3SiO_2$ glass, ca. 18% of SiO_4 units include at least two NBOs and the BO/NBO ratio is ca. 2.5 [16]. Using ^{29}Si NMR [22–24], the speciation of SiO_4 tetrahedra into Q_n units (where n is the number of BOs at the silicon) has been studied in much detail [22–25].

In Na trisilicate glass, the first peak in the Na–BO, Na–NBO and Na–Na distributions is at 0.27, 0.23 and 0.3 nm, respectively [13–19]. These numbers change little with the fraction of Na_2O. For other than Na^+ cations, the position of the first peak in the Alk–O distribution correlates with the ionic radius of Alk^+. For K and Cs silicates, these peaks are at 0.24 and 0.32 nm, respectively [15,17]. More details can be found in Refs. [10–30].

Alkali-deficient glasses are prone to phase separation and devitrification on a scale of 0.1–1 μm [31]. For Na_2O–Si_2O system, the region of im-

miscibility is between SiO_2 and $Na_2O \cdot 4SiO_2$; for Li_2O–SiO_2 system, it is between SiO_2 and $Li_2O \cdot 2SiO_2$ [31]. The phase separation is caused by slow cooling of the melt or prolonged heat treatment of the glass at 500–700°C. Although many glasses studied by EPR were in this immiscibility range, the effect of their morphology on the radiation damage has not been addressed.

2.2. Luminescence centers

Optical spectroscopy of alkali silicate glasses was discussed by Trukhin et al. [32–39]. Alkali silicate glasses are wide-gap oxides (the optical gap is 6–8 eV) which luminesce at 3–4 eV [32,33]. This emission can be stimulated by single-photon excitation above 5.5 eV [33–35], multiphoton excitation with UV [40–42], visible [39,43] and IR [44] lasers and by radiolysis [45–54]. Similar emission was observed in alkali-doped vitreous SiO_2 [32–35,50] and alkali monosilicate crystals (e.g., Li_2SiO_4) [53,54].

Optical spectra of silicate glasses systematically change with increase in the cation radius of the alkali modifier: the luminescence band shifts to the blue while the absorption and luminescence excitation bands shift to the red [53,54]. In alkali-doped vitreous silica, the lifetime of light-induced luminescence is shorter for larger alkali cations [36,37]. Doping sodium silicate glasses with alkali earth metals, Zn^{II}, Al^{III} and Ti^{IV} does not change their thermoluminescence spectra [47]. These spectra and the number of thermoluminescence peaks are virtually independent of the glass composition [47]. These results suggest that there is only one type of luminescence (L-) center in all of alkali silicate glasses of all compositions [32,33,53,54]. The modifier must be involved in these centers since the efficiency of intersystem crossing (radiative lifetime) correlates with the strength of spin–orbit interaction with the alkali atom [36,37]. From the studies on depolarization of the luminescence [32,33], it was decided that the L-center is formed: (i) by photoexcitation of the ground-state Alk–NBO complex and (ii) by recombination of shallow-trapped charges. This recombination is tunneling below 80 K and is phonon-assisted above 140 K [51,52].

Brekhovskikh and Tyul'kin [47] suggested that the excitation in the L-center is localized on the SiO_4 unit. Trukhin et al. [32,33,35,38] suggested that the L-center is the lowest triplet state of the Alk–NBO complex in which the Alk–O bond is partially covalent (a triplet $\equiv SiO^{\cdot\cdot}Alk$ biradical). This triplet state has slightly lower energy than the first excited singlet state of the same complex [32,38]. The two models are not mutually exclusive: the L-center could be the Alk–Q_3 complex in which the triplet excitation is localized on the Q_3 species perturbed by the crystal field of the alkali cation. Without the appropriate calculations, it is difficult to make a choice between these models.

2.3. Electron centers

Little is known about electrons trapped in band-tail and midgap states. The extension of the band-tails toward the midgap is 1–2 eV [35,48]. Mackey et al. [45] attributed absorption bands in irradiated silicate glasses to hole (H^+) and electron (E^-) centers depending on whether doping with Eu^{III} removed these bands from the UV–VIS spectra. In low-temperature Na silicate glasses, the $E^-_{1,2}$ bands centered at 2 eV are most prominent; these bands are shifted to 1.6 eV in K silicate glass [45]. Above 220 K, the $E^-_{1,2}$ bands anneal and two other bands, E^-_3 (4 eV) and E^-_4 (5.2 eV), appear. These two bands are stable below 500 K. Photoactivation of the E_{1-} center at 1–3 eV or its thermal activation above 40 K results in the L-center luminescence [45,53,54]. Photoactivation of hole centers at 2 eV results in the decay of the E^-_3 band [45].

The nature of *intrinsic* electron centers is not known. Frequently cited EPR observations of spin-1/2 electron centers [55,56] with g-factor of 1.96–1.97 were, actually, of the Ti^{III} impurity [57–59]. In these early EPR studies, the glass samples were made of naturally occurring silica (such as rock quartz and African sand) heavily contaminated with metal oxides. Upon radiolysis, octahedrally coordinated Ti^{IV} captures electron and forms a brightly colored spin-1/2 Ti^{III} center with $g \sim 1.95$–1.97 [57,58]. The $E^-_{1,2}$ bands observed by Mackey et al. [45] look much like the 2.5 eV band

of this Ti^{III} center [59]. It remains to be proven that these bands are from *intrinsic* centers.

It has been proposed that the E_1^- centers observed by Mackey et al. [45] are electrons trapped by isolated alkali cations [35,53,54,60]. This view is at odds with the energetics of electron trapping in amorphous SiO_2. Using conductivity methods, a sodium-related electron trap with binding energy of 2.4–2.5 eV was identified in the bulk of the SiO_2 layer on silicon [62]. The electron in the E_1^- center has binding energy of 1.2–1.5 eV [45]. It is too shallow a trap to be an alkali atom center. In addition, no such centers were found by EPR.

The only credible study on spin-1/2 electron centers is by optically detected magnetic resonance (ODMR) [60]. The ODMR signals were observed at 1.6 K; the L-center afterglow in $Na_2O \cdot 3SiO_2$ glass was used to detect tunneling recombination of charges in band-tail states. The ODMR spectrum consisted of a narrow resonance signal from an oxygen hole center (see below) and a broad bell-shaped signal centered at $g = 1.996$ with 23–25 mT fwhm. There is no evidence that this broad ODMR signal is from a band-tail electron; it could be from an impurity center or even a triplet state (i.e., the L-center itself). However, this signal resembles the EPR signal from alkali electron centers in sodium borate glasses [1,61]. These alkali cluster centers absorb at 1.5–2 eV [61], exactly where the $E_{1,2}^-$ bands were found.

It is well known that clusters of alkali cations are good electron traps. Spin-1/2 alkali clusters were observed by EPR in crystalline silicates (e.g., zeolites) and in alkali borate glasses [61]. Furthermore, Ag^0 atoms and Ag_2^+ clusters were observed by EPR in silver-doped alkali silicate glasses [32,63]. Nevertheless, in pure alkali silicate glasses, no paramagnetic alkali clusters or F-centers [64,65] were found by EPR. Thus, the alkali electron centers are either absent or diamagnetic. The second alternative is more probable. Perhaps, *the alkali electron centers in silicate glasses are negative-U defects.* (The electron correlation energy in a negative-U defect is so high that trapping the second electron is energetically favorable.) This second electron can come from an ionized midgap defect or a shallow band-tail state. This electron pairing could be inhibited only at very low temperatures. The resulting (diamagnetic!) electron centers are analogous to the M center in alkali halides [64,65].

2.4. Hole centers

The hole centers are readily observable by EPR. When they recombine with electrons, the light-emitting L-centers are formed [45–47]. Upon thermal annealing, the yield of the L-center emission correlates with the decay of the EPR signal from the hole centers [46]. Formation of hole centers and the L-center luminescence are inhibited by doping the glass with Ce^{III}, Eu^{III} [45,55,56,66,67] and oxides of As, Sb, Pb and Sn [47]. The hole centers are stable to 450 K [45].

There are two absorption bands from the hole centers, H_3^+ (2 eV) and H_2^+ (2.7 eV). The first band was correlated with spin-1/2 center OHC_2, the second with OHC_1 (see below). The H_3^+ center (OHC_2) is a deeper trap and has higher cross-section for electrons [45]. Reversible changes observed upon excitation of the H_2^+ center with 2 eV light suggest that the two hole centers are in thermal equilibrium [45,47]. Above 400 K, OHC_2 reversibly converts to an OHC_1-like defect [68]. Griscom [69] estimated that the activation energy of this conversion is 0.2 eV. This estimate is close to the activation energy of thermoluminescence [46].

2.5. EPR spectroscopy of hole centers

Oxygen hole centers were extensively studied by continuous-wave (cw) EPR [66–81] and, more recently, by pulsed EPR [82,83]. The subject was last reviewed by Griscom [68] (see also discussions in Refs. [69,71,80]).

In most of alkali silicate glasses, the EPR signals from OHC_1 and OHC_2 overlap spectrally. This overlap can be reduced either by changing the glass composition [75] or by microwave saturation of the OHC_1, which has longer spin–lattice relaxation times [69,77]. In glasses with $x \approx 15$–20 (where x is the mole fraction of SiO_2) the cw EPR signal is mainly from the OHC_1 [75], whereas in the glasses with $x \approx 1$–1.5, it is mainly from OHC_2 [70,71]. In K, Na and Li silicate glasses, the

relative yield of OHC_2 decreases linearly with x [75,81]. OHC_2 has the features of a radical with an axially symmetric g-tensor, while the OHC_1 has orthorombic g-tensor. In both cases, the principal values g_i of the g-tensor are distributed over a wide range, reflecting different environments in a disordered solid. The g_i values obey the following equation:

$$\Delta g_i = 2\lambda_i/\Delta, \tag{1}$$

where $\Delta g_i = g_i - g_e$, $g_e = 2.0023$ is the g-factor of a free electron, λ_i is the spin–orbit coupling constant and Δ is a splitting between the energy levels.

Studies of ^{17}O ($I = 5/2$) [71] and ^{29}Si ($I = 1/2$) [68,79] EPR satellites for OHC_1 in $K_2O \cdot 5SiO_2$ glass indicate that the spin density is located on the O 2p orbital of a single NBO. The spin density at the 3s orbital of the neighboring silicon (Si′) is 0.8%. Therefore, the OHC_1 is a $\equiv SiO\cdot$ radical formed by charge-compensation at the NBO (**I**).

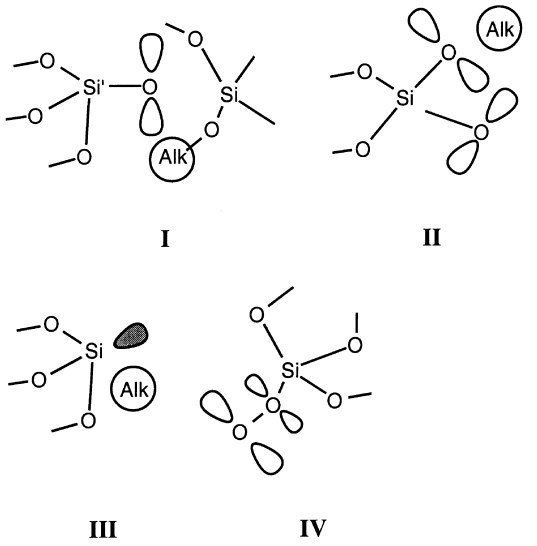

I **II**

III **IV**

Continuous-wave EPR spectra were simulated by averaging over all possible g_2 and g_3 values given by Eq. (1) while keeping $g_1 \approx g_e$; the resulting powder EPR spectrum was convoluted with a Lorentzian or Gaussian function. For OHC_1 in K [68,77] and Na [81] silicate glasses, this method gives good-quality fit of EPR spectra in 9 and 35 GHz bands. For OHC_1 in K silicate glasses, the distribution of Δs in Eq. (1) is Gaussian, with mean energy of 1.5 eV and fwhm ~ 0.7 eV [68]. Thus, in these glasses the main cause for the dispersion in the g_i values is *energetic* disorder. The reason for assuming that $g_1 \approx g_e$ is the planar symmetry of crystal field exerted by K^+: in center **I**, the NBO $2p_x$ (HOMO) orbital is perpendicular to the K–NBO–Si plane, with the g_1, g_2 and g_3 values corresponding to xx, yy and zz components of the g-tensor (the z axis is collinear with the Si–NBO bond). This simple approach is insufficient for simulation of EPR spectra for OHC_1 in Rb and Cs silicate glasses where the spin center has a subset of g_1 values well below g_e (Ref. [75] and this work).

The exact way in which the OHC_1 is formed and the degree to which it involves alkali cation(s) are unknown. There are two views: (i) that following the hole trapping, the compensating alkali cation migrates away from the Q_3 unit leaving uncompensated complex **I** [68] and (ii) that the compensating cation does not leave the trapping site and remains strongly coupled to the NBO [80]. There is also a possibility that the compensating cation is missing in the *precursor* of complex **I** making it a deeper Coulombic trap, as happens in borate glasses [1]. Since the linewidth of EPR spectrum from OHC_1 roughly correlates with nuclear dipole moment of the alkali cation, it was suggested that the broadening of the EPR spectrum is caused by electron-nuclear dipole–dipole interaction with a strongly coupled alkali cation [75,80,81]. Subsequently, this mechanism was shown to be insufficient to explain the observed line shapes and their variations with the type of the alkali cation [69]. Instead, it was suggested that the EPR line shape originated through rapid spin relaxation in the hole centers (in particular, for OHC_2) [69]. In the subsequent paper [70], it was concluded that this mechanism is not needed to explain the EPR line shape for OHC_2. In this work, we demonstrate that the spin relaxation is too slow to account for the observed broadening of resonance lines in both the hole centers.

In γ-irradiated 'wet' silica (fused silica with 1200 ppm of OH groups), there is an oxygen hole center that is related to the OHC_1 in alkali silicate glasses [72,73]. This center has different EPR parameters,

annealing behavior and optical properties than the oxygen hole center observed in neutron-irradiated 'dry' silica. The accepted wisdom is that in 'wet' silica the OHC is produced when a free triplet exciton interacts with the ≡SiOH group causing its scission. Since the siloxyl groups in silica are paired, it is reasonable to expect that the NBO in this hole center interacts with a proton on a neighboring siloxyl group; this interaction is lacking for OHC in 'dry' silica. This 'special interaction' model justified a similar model for the OHC_1 [68].

The hole center in 'wet' silica absorbs at 2 eV and emits at 1.9 eV [50,72,73]. This red luminescence was not observed in alkali silicate glasses [32,50]. In alkali-doped fused silica, a weak 1.9 eV band appears only when the irradiated sample is warmed to 300 K [50]. This behavior suggests that migration of compensating alkali cation from the hole center requires some thermal activation. Given that the alkali cation is coordinated with three-to-six BOs [10], this is not surprising. Furthermore, provided that Trukhin's model of the luminescence center in alkali-doped silica is correct, only OHC_1 in which the compensating alkali cation stays close to the NBO accounts for the formation of the L-center upon neutralization of the hole center. This is the reasoning behind the model of OHC_1 suggested by Kordas et al. [80].

Recently, the structure of the OHC_1 in ^{7}Li silicate glasses was studied with ESEEM [82] and HYSCORE (a 2D correlation pulsed EPR spectroscopy) [83]. With the first technique, it was shown that the OHC_1 is *weakly* coupled to several lithium cations [82], while the analysis of cross-peaks in HYSCORE spectra suggested that one of the lithium cations is *strongly* coupled to the electron spin ($a_{iso} \approx 0.5 \pm 0.1$ MHz, $T_\perp \approx 4 \pm 0.2$ MHz) [83]. In the point dipole approximation, this corresponds to the NBO–Li separation of 0.20 ± 0.02 nm and the spin density of 0.14% on the Li 2s orbital. Such a close association suggests that the compensating lithium cation does not leave the trapping site. In this EPR study, we provide additional evidence in favor of this model. (While this paper was reviewed, Astrakas and Kordas [84,85] published two more studies of OHC_1 in alkali silicate glasses. Using HYSCORE spectroscopy, they demonstrated that $^{23}Na^+$ is strongly coupled to OHC_1 in sodium silicate glasses (with $a_{iso} \approx 1 \pm 0.1$ MHz and $T_\perp \approx 1.8 \pm 0.2$ MHz) which indicates the NBO–Na separation of 0.23 ± 0.02 nm and the spin density of 0.11% on the Na 3s orbital [84]. These estimates agree well with the results obtained in our ESEEM study. Astrakas and Kordas [85] also suggested that the electron spin in OHC_1 is coupled to 13–24 distant alkali nuclei at ≈0.7 nm. Again, the existence of two subsets of alkali cations is supported in this work.)

In the OHC_1, the binding energy of the alkali cation is much lower than in a regular Q_3 unit. Therefore, accumulation of such hole centers should increase superionic conductivity of the glass. In the 'weak electrolyte' theory of conduction [26–28], the activation energy of cation migration $E_a \approx \Delta H/2 + E_m$ where ΔH is the enthalpy of the $\equiv SiO^-Alk^+$ dissociation and E_m is the 'true' activation energy of the migration (e.g., the elastic strain energy). Typical estimates of E_m are around 0.1 eV ($\sim E_a/5$) [26–28]. For alkali cations bound to OHC_1, we expect that $E_a \approx E_m$. The overall dc conductivity of irradiated glass would depend on the defect yield: generation of isolated hole centers may increase the conductivity but it would not change the activation energy of cation migration unless there is defect overlap. Experimentally, there are at least three regimes of superionic conduction in irradiated alkali silicate glasses. At low radiation doses (<5 kGy), the conductivity increases severalfold without much change in the activation energy of cation migration [86,87]. Further irradiation causes gradual decrease in the conductivity to the pre-irradiation level, possibly due to trapping of migrating Na^+ cations by electron centers [86,87]. However, prolonged irradiation (>10^{10} Gy) with 0.1–10 keV electrons causes structural changes that facilitate rapid migration of alkali cations [5–7,88–91]. According to Gedeon et al. [91] in this regime the concentration of the defects exceeds certain threshold so that there is a continuous conduction pathway for alkali cations across the sample. For sodium silicate glasses, this rapid migration occurs with $E_a \approx 0.05$ eV [88–90] as compared to $E_a \approx 0.5$–0.7 eV in non-irradiated glass [26–28]. We speculate that the

rapid migration of alkali cations might be due to the formation of chains of type-I hole centers.

OHC_2 is less characterized than the OHC_1. Many structural models for this center were considered (see discussion in Ref. [80]). At the present time, only the model developed by Cases and Griscom [70] is acceptable (structure **II**). This model rests on three observations: (i) axially symmetric OHC_2 can be reversibly converted to a broken-symmetry OHC_1-like center upon warming the sample [68,69], (ii) the observed ^{17}O satellite structure suggests that the spin density is shared between two magnetically equivalent NBOs (although the quality of the cw EPR data is insufficient to make this statement with certainty, due to the presence of EPR signals from other spin centers and Cu^{II} impurity) [70] and (iii) the spin density on ^{29}Si is comparable to that on ^{29}Si in OHC_1 [70].

Cases and Griscom [68,70] suggested that in the OHC_2, the spin is shared between two NBO 2p orbitals lying in the NBO–Si–NBO plane; the alkali cation is out of this plane. Upon thermal activation, the cation migrates into the plane and the unpaired electron localizes on a single NBO [68]. The OHC_2 can be visualized as a hole trapped on the Q_2 species with one of the compensating alkali cations missing. The remaining alkali cation either couples to a single NBO (yielding an OHC_1-like defect) or migrates away (yielding OHC_2). In the latter case, the g-tensor of the symmetric OHC_2 is orthorombic, with g_1 and g_3 values given by $\Delta g_1 = 2\lambda/\Delta\cos^2(\theta/2)$ and $\Delta g_3 = 2\lambda/\Delta\sin^2(\theta/2)$, where θ is the NBO–Si′–NBO angle [70]. It was assumed that the angle θ is within $\pm 15°$ from the regular BO–Si–BO angle and $\theta \propto \Delta^{-1/2}$. Given many assumptions made in this model, it is difficult to conclude decisively that the two NBOs are magnetically equivalent. As shown in this work, this equivalence must be a result of rapid dynamic averaging between the OHC_1-like conformers.

2.6. Other radiation-induced spin-1/2 centers

In addition to the hole centers, there is a silicon dangling bond center (**III**) and several O-centered radicals (e.g., **IV**). The dangling bond center (called E′ in analogy to a similar E'_γ center in fused silica) gives a narrow EPR line at $g \approx 2$. The related ^{29}Si–E′ center exhibits a 37 mT doublet [71]. Since the hyperfine coupling constant (hfcc) for ^{29}Si in the E′ center is 12% lower than the hfcc in the E'_γ center [63,72,73] (37 vs. 42 mT), it was speculated that the spin density is shared with a nearby alkali cation [71].

When γ-irradiated K silicate glass is annealed at 540 K, the hole and E′ centers decay and the residual EPR signals are from radicals whose cw EPR spectra, ^{17}O and ^{29}Si satellite structure and microwave saturation behavior are similar to those of the silicon peroxy radical (Si-bonded $O_2^-\cdot$) in fused silica (**IV**) [71]. After annealing at 580 K, this EPR signal disappeared, and a weak residual signal from a radical with a more symmetric g-tensor was observed. This radical was identified as the interstitial superoxide anion ($O_2^-\cdot$) with $A(^{29}Si) \approx 0$. In $K_2O \cdot 1.3SiO_2$ glass annealed at 610 K, an additional narrow EPR signal from ozonide anion, $O_3^-\cdot$, was observed [71]. In O^+ implanted soda lime glass, interstitial $O\cdot^-$ ions were found [92]. Thus, at least three kinds of oxygen interstitial centers were found in irradiated alkali silicate glasses. It has been guessed that these species are related to radiolytic O_2 in alkali silicate glasses [2]. Indeed, in fused silica, where only bonded peroxy radicals were observed [63], no evolution of molecular O_2 was found [5–7].

The mechanism for formation of these O-centered radicals is unknown. Cherenda and Yudin [76] suggested that in vitreous silica and alkali silicates, the peroxy radicals and hole centers are formed upon homolysis of peroxy linkages (≡Si–OO–Si≡). For silica, this view has long been discredited [63]. In γ-irradiated fused silica, the E'_γ centers and peroxy radicals are formed through hole trapping at oxygen vacancies (≡Si–Si≡) and peroxy linkages, respectively [63,72,73]. The decay of Frenkel pairs (dissociated self-trapped triplet excitons) also leads to these defects [93]. Above 500 K, the E'_γ centers convert to peroxy radicals in a reaction with interstitial O_2 [94–96]; the reverse reaction requires electron excitation of the peroxy radical [97,98]. Since EPR observation of O_2-related spin centers in alkali silicate glasses required thermal annealing above

550 K [71], it is not clear which one of these mechanisms operated in these glasses.

In addition to the intrinsic centers examined above, various transition metal impurity centers have been identified (see Ref. [63] for a review). Interestingly, despite 100–300 ppm of siloxyl groups present in the glass, trapped H atoms are not observed in alkali silicate glasses.

In conclusion, much is to be learned about radiation damage in alkali silicates. Of all radiation-induced centers in these glasses, only OHC_1 and L-centers are understood in some detail. These centers were related to the Alk–NBO complex and to each other. The mechanism for the OHC_1 formation and its general structure are not fully understood. Proposed structures for the hole and luminescence centers are sketchy. A feasible model for OHC_2 was proposed, but it needs further elaboration and experimental support. Several oxygen interstitial and vacancy centers were identified, but their formation mechanisms and relation to interstitial O_2 are unknown. The nature of electron centers in silica and alkali silicate glasses is as enigmatic as ever.

3. Experiment

3.1. Sample preparation

Glass samples were prepared under oxidizing conditions, by melting 5–10 g batches of alkali carbonates mixed with crushed Suprasil II, in corundum crucibles. The mixture was first warmed to 600°C over 1/2 h and then heated to 1400–1600°C for 1–3 h. For some compositions (low molar fraction of alkali), this procedure gave an opaque ceramic solid; in such cases, the samples were melted for 30 min in the flame of a propane-oxygen torch. All the samples used in this work were clear glassy solids. The samples were stored in a desiccator and crushed under nitrogen. In the following, the samples are referred to as Alk-x, where Alk is the type of alkali cation and x is the SiO_2/Alk_2O ratio.

Al^{III} doped glass was prepared by addition of alumina, Ti^{IV} doped glass – by addition of $(NH_4)_2TiO(C_2O_4)_2 \cdot H_2O$. Ce^{III} doped glass was prepared under reducing conditions; CeO_2 was used as a source of cerium and sucrose as a reducing agent. The reduction of Ce^{IV} was complete by >95%, as determined by UV–VIS spectroscopy.

Using other siliceous materials than suprasil II (e.g., high-grade SiO_2 from Aldrich) resulted in contamination of samples by Al^{III}, Ti^{IV} and Cu^{I}. After irradiation, these samples gave EPR signals from Cu^{II} and Ti^{III} ions. Some suprasil batches were found to yield strong EPR signals from Al hole centers; careful screening of silica batches was needed to find a suitable source of pure SiO_2. Even our best samples had significant Fe and OH impurity (100–300 ppm); this level of contamination is typical for other 'pure' silicate glasses [99]. The Fe^{II} and Fe^{III} impurity can be observed in cw EPR spectra (broad resonance signals at $g_{\mathrm{eff}} \approx 2$ and $g_{\mathrm{eff}} \approx 4.3$) and near-IR spectra ($Fe^{II}$ only), the OH impurity – by IR spectroscopy. Outgassing the glass samples at 500–600°C yields $\sim 10^{16}$–10^{17} cm^{-3} of H_2O, CO_2 and N_2. Thus, the 'purity' of our samples is relative. While the EPR signal from Ti^{III} does not overlap with the EPR signals from the intrinsic spin centers, the signal from Cu^{II} overlaps with the EPR signals from peroxy/superoxide radicals and OHCs; the identity of the impurity center can be established by studying its relaxation and annealing behavior. No aluminum-related centers were observed even in intentionally Al-doped glasses (<1 wt%).

The samples were irradiated using γ-rays form a ^{60}Co facility (10 kGy/h) or 3 MeV electrons from a Van de Graaff accelerator (Chemistry Division, Argonne National Laboratory). In the latter case, the target was either water-cooled (for 300 K irradiation, 9×10^8 Gy/C) or liquid N_2 cooled (for 77 K irradiation, 5×10^7 Gy/C). The electron current was varied between 0.5 and 10 μA. The warming of the sample during the irradiation was within 2°C. When 3 MeV electrons were used, the EPR spectra were obtained 1–2 min after irradiation. Typical doses were ranging from 0.1 kGy to 10 MGy; if not stated otherwise, the samples were irradiated to 0.65 MGy at 300 K.

The crushed glass samples were vacuum-sealed in 4 mm Suprasil II tubes. The upper part of the sample tube was shielded from the irradiation; as an addition guard the tip was flame annealed at

1200°C, and the tube flipped. No EPR signals from the annealed sample tube was observed.

3.2. Continuous-wave EPR and ENDOR

First-derivative cw EPR spectra were obtained using 100 kHz modulation. At 4–50 K, the T_1 relaxation of the OHCs is sufficiently long to cause slow-passage distortion of the cw EPR signal. Furthermore, a broad EPR signal from Fe^{III} at $g_{eff} \approx 2$ overlaps with resonance signals from intrinsic spin centers. At 4.7 K, the OHC_1 in K silicate glasses saturated at 5 mW and Cs glasses showed partial microwave (μw) saturation, whereas Li and Na glasses showed no μw saturation even at 100 mW. The saturation of the signal from the E′ center requires 1–10% of the μw power needed to saturate OHC_1. Except for the relative yield of the narrow signal from the E′ center (which overlaps with EPR signals from the hole centers), the cw EPR spectra of the hole centers obtained for different radiation doses are identical.

The spin concentrations were obtained by double integration of the first-derivative EPR spectra obtained at low μw power; the integral was calibrated relative to the EPR signal from a weak pitch sample (10^{13} spins/cm) and $CuSO_4 \cdot 5H_2O$. The g-factors were calibrated vs. DPPH radical.

Continuous-wave ENDOR spectra in the X-band were obtained on a Bruker ESP300E spectrometer at the laboratory of Professor M. Makinen, University of Chicago; the Q-band (35 MHz) spectra were obtained by Dr J. Telser of Roosevelt University on a home-built ENDOR spectrometer. The X-band spectra were obtained at 4–10 K using μw power of 20 mW, maximum radio-frequency power, FM at 12. 5 kHz and FM depth of 50 kHz. The Q-band spectra were obtained at 2 K, 2 G modulation, using the μw power of 20 W.

3.3. Pulsed EPR

Electron spin echo (ESE) spectra were obtained at 8.5–9.2 GHz using a home-built pulsed μw bridge. Below 300 K, the temperature was controlled using a Helitran cryostat. Between 300 and 600 K, hot air was blown through a sapphire jacket containing the sample tube.

Short 20–30 ns microwave pulses were used for excitation of the spin centers. Longer μw pulses (up to 200 ns) were used to obtain field-swept ESE spectra with resolution better than 0.1 mT. Primary (90°-τ–180°-τ) and stimulated (90°-τ–90°-T–90°-τ) spin echo was observed as a function of the delay times τ and T. Prefixes 'p' and 's' will be used to distinguish between the two kinds of the spin echo. Inversion-recovery (180°-T–90°-τ–180°-τ) sequences were used to study spin–lattice relaxation; virtually the same kinetics were obtained from the sESE kinetics. The dead time of the spectrometer was between 180 and 250 ns, depending on the dielectric load. For convenience, the field in the EPR spectra are given in the units of effective g-factors defined as $g_{eff} = \omega/\beta_e B_{res}$, where B_{res} is the resonance field, ω is the μw frequency and β_e is the electron magneton.

In the absence of echo modulation by magnetic nuclei, the pESE kinetics in the τ domain were exponential, $E(\tau) = \exp(-2b\tau)$. The phase memory time T_p of the spin packet was defined as $T_p = 1/b$. The decay parameter b of θ_p-τ–$2\theta_p$-τ primary echo depended on the flip angle θ_p of the excitation μw pulse. For instantaneous spin diffusion caused by dipole–dipole interaction of uniformly distributed electron spins

$$b = b_0 + 4\pi^2/9\sqrt{3}(g_e\beta_e)^4 N_s \sin^2(\theta_p/2), \qquad (2)$$

where N_s is the density of spin centers. Eq. (2) was used to determine local spin densities for hole centers.

4. Results

4.1. High-temperature regime (>250 K)

Fig. 1(a) shows a family of field-swept pESE spectra obtained from irradiated K-3 glass (300 K). These spectra were obtained as a function of the delay time τ between the 90° and 180° μw pulses and normalized to the same value at $g_{eff} \approx 2.015$. Since the amplitude of the pESE signal for a given delay time τ is proportional to $\exp(-2\tau/T_p)$, the spin packets with longer T_p

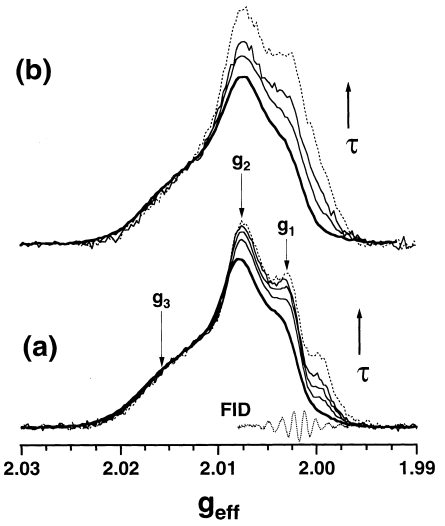

Fig. 1. Field-swept pESE spectra from irradiated K-3 glass. The spectra were observed at 300 K (a) and 420 K (b) for μw frequency of 8.54 GHz, repetition rate of the pulse sequence of 5 kHz, and exception (90°) μw pulse of 35 ns. The spectrum indicated 'FID' is from the E′ center; this spectrum was obtained by boxcar integration of the free induction decay at 0.2–0.3 μs following a 20 ns, 90° μw pulse (the oscillation in the field domain are due to transient nutation of electron spin in the time domain; the nutation frequency depends on B_0). Three centroids g_i of the g-tensor envelope are indicated in traces (a); the side line at $g_{\text{eff}} \approx 2$ is the echo signal from E′. The spectra for different delay times τ were normalized to the same amplitude at $g_{\text{eff}} \approx g_3$. The spectra were obtained for $\tau = 0.3$ μs (bold lines), 0.45, 0.65, 0.85 and 1.25 μs (dashed lines).

(higher b) yield stronger echo signals at later delay times. According to Fig. 1(a), the hole centers with $g_{\text{eff}} > 2.01$ have longer phase memory times than those with $g_{\text{eff}} < 2.01$.

The narrow pESE signal at $g_{\text{eff}} \approx 2$ is from the E′ center; this center has phase memory time $T_{\text{p}} \approx 1.03$ μs and spin–lattice relaxation time $T_1 \approx 120$ μs (at 300 K). The T_1 time varies little (10–15%) with the radiation dose and alkali modifier fraction; very similar T_1 times were obtained for E′ centers in Li and Na silicate glasses. The broad signal with g_{eff} between 1.99 and 2.025 is from the OHC_1 (due to rapid T_2 relaxation, pESE signals from OHC_2 cannot be observed at 300 K). The decay kinetics of pESE as a function of τ and sESE kinetics as a function of T are both exponential, in any resonance field. The peaks at $g_{\text{eff}} \approx 2.003$, 2.0076 and 2.015 roughly correspond to centroids of the $\{g_i\}$ distribution (Fig. 1(a)). In the corresponding resonance fields, the T_{p} and T_1 relaxation times are, respectively, 0.66 and 1.91 μs (g_1), 0.64 and 1.83 μs (g_2), 0.6 and 2.14 μs (g_3). *Thus, the relaxation times are shorter for lower-field (higher-g_{eff}) signals.* For T_1 times, this is true for both types of hole centers, in all glasses, at any temperature. Fig. 2(a) shows the dependence of the decay parameter b as a function of g_{eff}. This parameter is independent of g_{eff} for $g_{\text{eff}} > 2.018$ and increases linearly with g_{eff} between 2.005 and 2.0018 (dashed line in Fig. 2(a)). At $g_{\text{eff}} < 2.005$, the pESE signals from the OHC_1 and E′ centers overlap, and the observed T_{p} times become longer (Fig. 2(a)). When the flip angle dependence of the decay parameter b was obtained, formula (2) was found to held for spin packets with $g_{\text{eff}} > 2.005$.

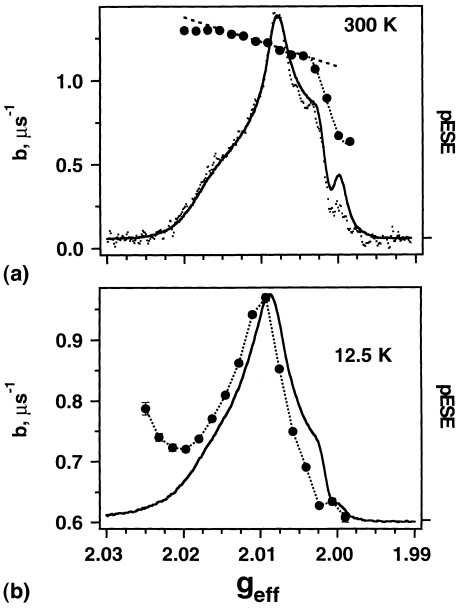

Fig. 2. Field dependences of the decay parameter b of the primary spin echo ($b = 1/T_{\text{p}}$) for the same irradiated K-3 sample, observed at 300 K (a) and 12.5 K (b) (filled circles). The echo signals were excited selectively, using 50 ns μw pulses (repetition rate was 5 kHz at 300 K and 1 kHz at 12.5 K). Bold traces are normalized field-swept pESE spectra obtained at $\tau = 0.3$ μs. In (a), a pESE spectrum from the same sample annealed for 5 min at 340 K is shown by dots (this signal was amplified 12 times). In this spin-dilute sample, the pESE spectrum looks the same way as the spectrum in the pre-annealed sample.

While the local spin density N_s correlated with the radiation dose, b_0 was dose-independent but g_{eff}-dependent (increasing from 0.3 to 0.5 μs^{-1} across the spectrum). The concentrations N_s inferred from Eq. (2) and those determined by integration of cw EPR spectra were within a factor of 2 from each other (N_s varied from 10^{17} to 2×10^{18} cm^{-3} with the radiation dose). Thus, the hole centers are uniformly distributed, at least on the scale exceeding 1 nm. Even for the highest spin concentrations, the effect of dipolar broadening on the appearance of pESE and cw EPR spectra is negligibly small (compare the two traces in Fig. 2(a)).

Since the T_1 times for OHC_1 and E′ centers differ by more than an order of magnitude, the signals from OHC_1 can be eliminated by observing sESE at sufficiently long delay times T between the second and third microwave pulses (Fig. 3(a)). For $T > 15$ μs, the field-swept sESE spectra are from the E′ center only. Fig. 3(b) shows these spectra for K-3 and Na-3 glasses. The sESE signal from K-3 is centered at $g_{eff} = 1.9996$ and has Gaussian shape with $\sigma = 0.24$ mT (the first derivative peak-to-peak width $\Delta B_{pp} = \sqrt{2}\sigma$); the ESE signal from Na-3 is 70% broader and the corresponding g-tensor is axially symmetric ($g_\perp \approx 1.9996$ and $g_\parallel \approx 2.005$). In K silicate glasses, the excitation of the E′ center with a single 90° μw pulse yields free-induction decay (FID) lasting over a microsecond (Fig. 1(a) shows field-swept EPR spectrum obtained by time window integration of this FID signal). Therefore, for E′ center in K silicate glasses there is almost no inhomogeneous broadening of the EPR signal. [1] In Na and Li silicate glasses, the signal from the E′ center is inhomogeneously broadened. The observation of FID for E′ center in K glasses is incompatible with the g-factor analysis given in Ref. [71]. It is likely that in this cw EPR work, the resonance signal from the E′ center was not sufficiently separated from the overlapping signal from hole centers.

[1] Inhomogeneous broadening is caused by spectral overlap of resonance signals from differently oriented spin centers with asymmetric g-tensor. Homogeneous broadening is due to T_2 relaxation in these centers. With spin echo detection, the homogeneous broadening is transferred to the time domain. Inhomogeneously broadened lines do not yield FID signals.

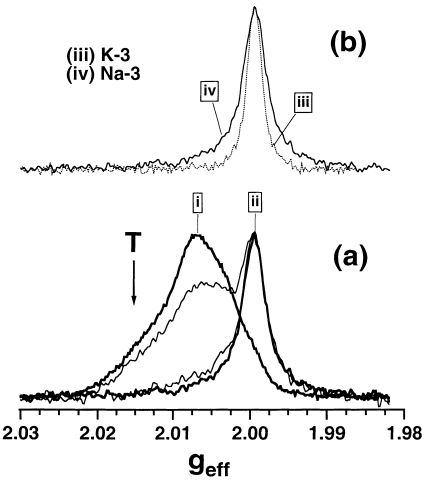

Fig. 3. Field-swept sESE spectra from irradiated Na-3 glass for $\tau = 0.3$ μs and $T = 0.6$, 5, 15 and 30 μs at 300 K (a). With increase in the delay time T, the weight of the sESE signal from OHC_1 (i) decreases while the weight of the E′ signal (ii) increases. The T_1 times for spin packets (i) and (ii) are 1.7 and 140 μs, respectively; the weights of the sESE signals decrease with T as $\exp(-T/T_1)$. (b) Normalized $T = 30$ μs traces observed in (iii) K-3 and (iv) Na-3 glasses; these signals are from E′ centers only.

Due to high sensitivity of pulsed EPR, the observation of certain ^{29}Si satellites does not require isotope enrichment of the glass. Fig. 4(a) shows a wide-swept pESE spectrum from irradiated Na-3 glass. Apart from a 'narrow' signal at the center (from OHC_1 and E′), there is a signal from Ti^{III} impurity at $g_{eff} \sim 1.95$–1.97 and a set of two lines (at 0.1% of ESE signal from the OHC_1) whose centers are separated by 36 ± 1 mT. Apparently, this is the same ^{29}Si–E′ doublet observed by cw EPR in K-5 glass by Cases and Griscom [71] and K-13.3 glass by Cherenda et al. [100]. Thus, the orbital structure of the E′ defect in sodium and potassium silicate glasses is virtually the same, the only difference being axiality of the g-tensor for E′ center in Na glasses. This similarity cannot be explained if there is sharing of spin density between Si and a nearby alkali cation, as suggested by Cases and Griscom [71].

The EPR signal from E′ centers is more prominent in alkali-deficient glasses and at higher radiation doses. While the concentration of OHC_1 stabilizes at ca. 5×10^{18} cm^{-3} at the dose of

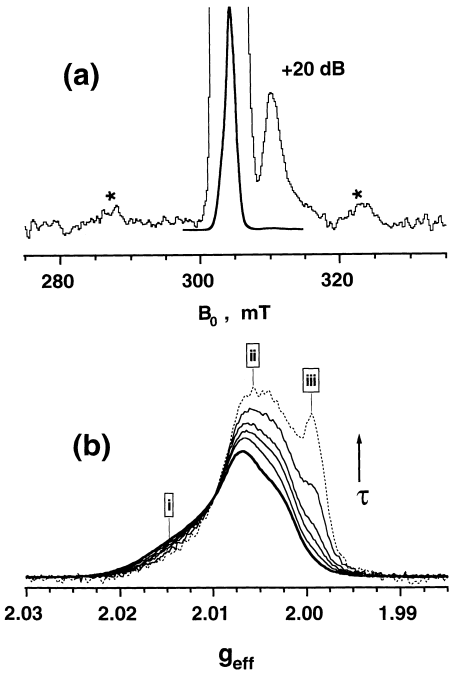

Fig. 4. Field-swept pESE spectra from irradiated Na-3 glass. The spectra were obtained at 300 K (a) and 355 K (b), respectively (8.54 GHz, repetition rate 5 kHz, 27 ns pulse). (a) Wide-scan pESE spectrum showing signals from Ti^{III} impurity centers (a singlet at 310 mT with $g_{eff} \approx 1.97$) and a doublet from ^{29}Si–E′ center (indicated with asterisks). 10^5 echo signals were averaged to obtain this spectrum. The signal at the center is from OHC_1 and ^{28}Si–E′ center. (b) Evolution of the pESE spectrum in the τ domain, $\tau = 0.25$ μs (bold trace), 0.45, 0.65, 0.85, 1.25 and 1.65 μs (dashed trace). The traces were normalized at $g_{eff} \approx 2.01$. Phase memory times T_p for spin packets (i)–(iii) are 0.53, 0.63, and 1 μs, respectively. Growing signal (iii) is from the ^{28}Si–E′ center.

10–100 kGy, the concentration of E′ centers steadily increases to at least 5 MGy (at 300 K). The yield of E′ centers does not change significantly upon doping the glasses with Ce^{III}.

At higher temperatures (300–480 K), the pESE spectra do not change much (Figs. 1(b) and 4(b)). Phase relaxation is faster at higher temperatures. At 450 K, the phase memory times for OHC_1 in K-3 shorten by 30% as compared to the T_p times at 300 K. Another trend is an increase in the spread of phase memory times across the ESE spectrum (the ratio of the shortest to the longest T_p times increases from 9:10 at 300 K to 3:4 at 450 K); the dependence of b on g_{eff} still resembles the one shown in Fig. 2(a).

Alkali-deficient silicate glasses are known to phase-separate upon prolonged heat treatment. Two Na-19 glasses, one as-made and another annealed for 1 h at 800 K, were irradiated to 0.2 MGy at 300 K. Although the EPR signals from OHC_1 were identical in both these glasses, in phase-separated glass the T_p time was ca. two times shorter. The flip-angle dependences indicated that this shortening was due to higher local concentration of hole centers in the phase-separated glasses. Therefore, hole traps in Na-rich islands are deeper than hole traps in the Si-rich phase. The T_1 times for a subset of E′ centers in phase-separated glass were by an order of magnitude longer than in homogeneous glass, approaching the T_1 times for E'_γ defect in silica. Perhaps, the E′ centers are preferentially formed in the Si-rich phase. Thus, microscopic inhomogeneity of the glass leads to inhomogeneity of radiation damage. This applies to other glasses: In alkali borosilicate glasses, the glass morphology has the major effect on the spatial distribution of radiation-induced defects [101].

4.2. Intermediate temperatures (50–200 K)

In K-3 glasses cooled below 160–180 K, the spin relaxation pattern for OHC_1 differs from that observed at 300 K (Fig. 5). Whereas at higher temperatures the high-field signals have shorter T_p times than the low-field signals, at lower temperatures the spin packets at the center of the EPR spectrum relax faster than those in the wings. This transformation is complete at 30–40 K. Below 30 K, the g_{eff} dependence of the relaxation rates b reproduces the g_{eff} dependences of the pESE signal itself (Fig. 2(b)); the corresponding phase memory times are 2–3 times longer than T_p times for the same sample at 300 K.

Even more dramatic are changes in the time scale of spin–lattice relaxation. Below 100 K, the inversion-recovery and sESE kinetics are no longer exponential; these kinetics can be fit with stretched-exponential dependence, $\exp(-[T/T_s]^\alpha)$, with α between 0.5 and 1. At 100 K, $\alpha \approx 0.8$ and $T_s = 23$ μs (g_3 centroid) and 12 μs (g_2 centroid); the

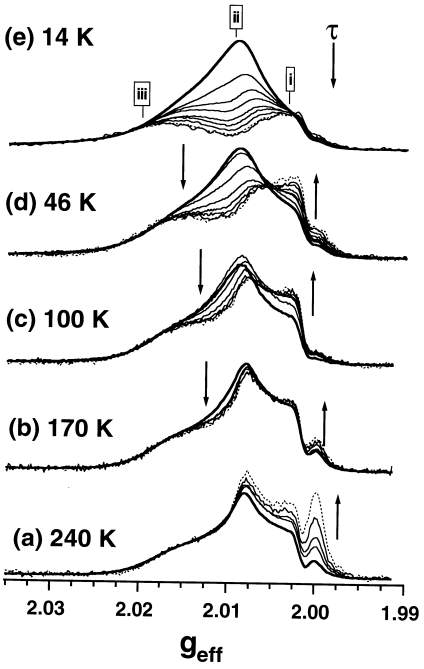

Fig. 5. The sets of field-swept pESE spectra from irradiated K-3 glass obtained for different delay times τ. The spectra were observed at the temperatures indicated, at 9.07 GHz using a 50 ns, 90° μw pulse. The repetition rate was 5 kHz (a, b), 1 kHz (c), and 0.2 kHz (d, e) respectively. The spectra were normalized at $g_{\text{eff}} = 2.018$. The delay times τ were 0.25 μs (bold traces), 0.6, 1, 1.5, 2 and 2.5 μs (b–e), 3 μs (c–e), 3.5 μs (d, e) and 4.2 μs (e). The dashed traces correspond to the maximum τ time. The signal at $g_{\text{eff}} \approx 2$ is from E′ center; in low-temperature pESE spectra this signal saturates due to high repetition rate of the pulse sequence. The trends with increasing τ are indicated with arrows. At 14 K, the spin memory times T_p for spin packets (i)–(iii) are 1.5, 1.1, and 1.7 μs, respectively.

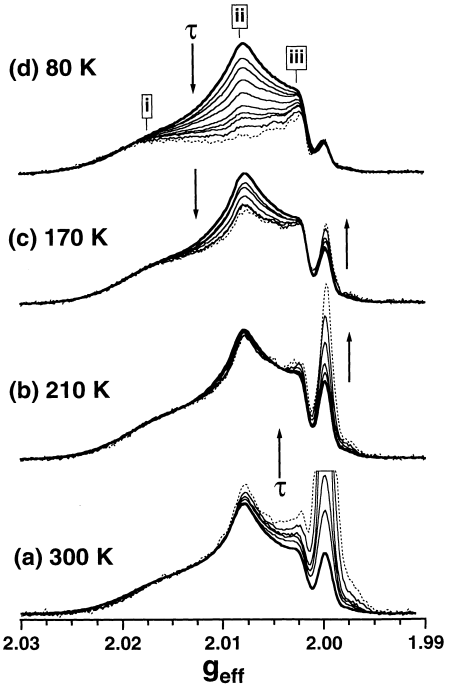

Fig. 6. Sets of field-swept pESE spectra from K-19 glass obtained for different delay times τ. The sample was irradiated at 300 K. The spectra were observed at temperatures indicated in the figure at 9.07 GHz using 55 ns excitation μw pulse. The repetition rate was 5 kHz. The spectra were normalized at $g_{\text{eff}} = 2.018$. The delay times τ were 0.45 μs (bold traces), 0.65, 0.85, 1.25 and 1.65 μs, 2.05 μs (b–d), 2.45 μs (c, d), and 2.85, 3.25 and 4.25 μs (d). The dashed traces correspond to the maximum τ time. At 300 K, the spin memory times T_p for spin packets (i)–(iii) are 0.7, 0.73, and 0.76 μs, respectively; at 80 K – 1.64, 1.25, and 1.54 μs, respectively.

T_p times for these signals are comparable (1.1–1.2 μs) and $b_0 \approx 0.7\ \mu s^{-1}$. Below 50 K, $\alpha \approx 0.5$ and the T_s times increase dramatically. At 45 K, the T_s times for these two centroids are 35 μs (g_3) and 20 μs (g_2); at 14 K −280 μs (g_3) and 145 μs (g_2). Below 10 K, the decay of pESE is no longer exponential, this is possibly due to low-frequency echo modulation by ^{39}K nuclei.

The turnover of relaxation behavior for OHC_1 was also observed in K-19 glass at 190 K (the temperature of the turnover depends on the spin density of hole centers). The transformation of the pESE spectra followed different pattern from the hole centers in K-3 glass (Fig. 6). In the K-19 glass, the pESE spectra of hole centers obtained at $\tau \approx 0.2$–0.3 μs did not change between 5 and 350 K. In the K-3 glass, these spectra underwent a dramatic change between 40 and 100 K.

Apparently, both types of oxygen hole centers, OHC_1 and OHC_2, were observed in the low-temperature K-3 glass. At 300 K, the T_p time of OHC_2 is shorter than the dead time of the spectrometer, and its echo signal is missing in the pESE spectra. At lower temperatures, the OHC_2 relaxes less rapidly, and the ESE spectra are both from the OHC_1 and OHC_2. To demonstrate this, we studied K-1.3 glass that yields cw EPR signal from just one kind of hole center, OHC_2 [70] (Fig. 7(a)). The pESE signal was observed only below 175 K.

Between 5 and 175 K, the decay parameter b linearly increases with temperature: $b\ (\mu s^{-1}) \approx 0.95 + 8.2 \times 10^{-3}$ T (for $g_{eff} \approx 2.01$ signal). This increase corresponds to a very low activation energy <10 meV. Under identical conditions (temperature and spin density), the phase relaxation in OHC_2 (in K-1.3 glass) is 2–4 times faster than in OHC_1 (in K-3 and K-19 glasses). More pronounced is the difference in the spin–lattice relaxation times: At 65 K, the T_s time for OHC_2 in K-1.3 glass is 0.5 vs. 45 μs for OHC_1 in K-19 glass (for the spin packet at the center of the pESE spectrum). Though the spin–lattice relaxation in OHC_2 is rapid, it is not fast enough to explain homogeneous broadening of cw EPR lines as suggested by Griscom [69]. Note that the times T_s for OHC_2 are within a factor of 0.5–2 from the T_p times at the same temperature. Equal T_1 and T_2 times are typical for relaxation dynamics with short correlation time, e.g., spin–rotation relaxation. *It appears that a very fast, activation-less dynamics is occurring in the OHC_2.*

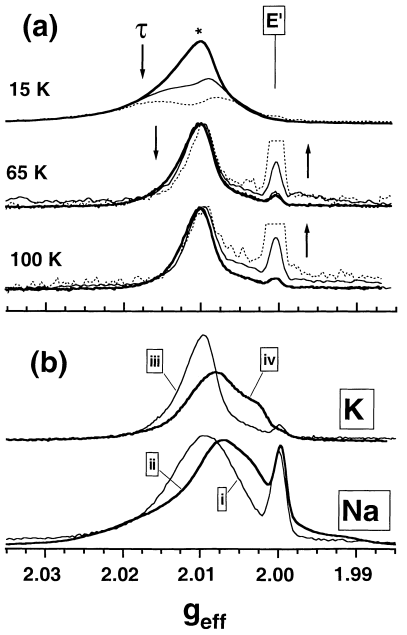

Fig. 7. (a) Field-swept pESE spectra from K-1.3 glass irradiated to 36 kGy at 77 K. The spectra were observed at temperatures indicated in the figure using 30 ns excitation μw pulse. The repetition rate was 1 kHz; the spectra were normalized at $g_{eff} = 2.018$. The delay times τ were 0.3, 0.4 and 0.8 μs (65 and 100 K) and 0.3, 1.3, and 2.3 μs (15 K). The signal marked with an asterisk is from OHC_2. (b) Comparison between the shapes of pESE spectra from irradiated (i) Na-1.3 and (ii) Na-19 glasses (vide infra) and (iii) K-1.3 and (iv) K-3 glasses (vide supra). The glass samples were irradiated at 77 K; pESE spectra were observed at 65 K for $\tau = 0.3$ μs. The signals at $g_{eff} \approx 2$ are from E′ centers.

Since between 100 and 450 K the relaxation times for OHC_2 are short, the evolution of field-swept pESE spectra observed in this temperature range cannot be explained by the interference from the OHC_2. Rather, this evolution originates in the peculiarities of T_2 relaxation in OHC_1.

Hole centers in ^{23}Na glasses have shorter relaxation times than the centers in ^{39}K glasses and exhibit modulation of ESE envelope due to dipole–dipole interaction with magnetic ^{23}Na nuclei (ESEEM). Apart from the ESEEM, the relaxation *patterns* for hole centers in K and Na silicate glasses of the same composition are quite similar. There is only one difference: in Na glasses the turnover in the relaxation behavior for OHC_1 was observed at much lower temperatures than in K glasses: 80–100 vs. 170–200 K. Whatever atomic motion contributed to the T_2 relaxation in OHC_1, it requires less thermal activation for smaller alkali cations. The field-swept pESE spectra of hole centers in K and Na glasses are similar, but the spectral envelope in Na glasses is broader, both for OHC_1 and OHC_2 (Fig. 7(b)). Since with the echo detection the homogeneous broadening is transferred to the time domain, Fig. 7(b) indicates that in sodium glasses the $\{g_i\}$ values are more disperse than in potassium glasses. Spin relaxation has no effect on the shape of cw and echo EPR spectra for OHC_1 and OHC_2.

It is worth commenting that in some spectra shown in Figs. 5–7, the $g_{eff} \approx 2$ signal from E′ centers is weak. This is due to long spin–lattice relaxation time for this center at cryogenic temperatures (below 10 K, $T_s > 1$ ms). Unless the repetition rate of the pulse sequence is lower than several Hz, the magnetization does not fully relax between the excitation pulses causing saturation of the EPR transition. Using low repetition rates restores the ESE signal to full magnitude but lengthens the acquisition. When low-rate sampling is used, a strong signal from the E′ center was always observed, even in alkali-loaded glasses

($x < 2$) for which these centers were reported missing [70].

4.3. Low temperatures (<30 K)

Below 30–40 K, the evolution of pESE spectra in the time (τ-) domain follows the pattern shown in Figs. 5(e) and 6(d): the stronger echo signal relaxes faster. In Fig. 2(b), the spectrum is superimposed with the field dependence of the decay parameter b of the primary echo for K-3 glass at 12.5 K. For $g_{\text{eff}} > 2.02$, these two curves closely resemble each other. The same patterns were observed for K-19 glass (where the echo signal is from OHC_1) and for K-1.3 glass (where the echo signal is from OHC_2).

This behavior can be explained using Eq. (2). Since the μw pulse has finite duration t_p, in a given field B_0 only spin packets that have resonance fields sufficiently close to the B_0 field ($|\omega - g_{\text{eff}}\beta_e B_0| < t_p^{-1}$) are excited by this pulse. Thus, the spin density N_s in Eq. (2) is the concentration of spin centers for which $|B_{\text{res}} - B_0|$ is $<10^{-4}$ T (the 90° pulse was 50 ns long). In the absence of hyperfine structure, the concentration of spin centers with $B_{\text{res}} \approx B_0$ is proportional to the amplitude of the EPR signal at B_0, which explains the behavior shown in Fig. 2(b). *The evolution of pESE spectra in the time domain is due to instantaneous spin diffusion* (*driven by electron dipole–dipole interaction of nearby spin centers*) *under selective μw excitation.*

For $g_{\text{eff}} < 2.02$, the relaxation behavior cannot be explained in this way. Close examination of the low-field part of the pESE spectrum (Fig. 8(a), trace (i)) shows that there is another resonance signal (a shoulder extending down to $g_{\text{eff}} \approx 2.1$) that overlaps with the resonance signal from the hole centers. This signal is 50–200 times weaker than the signal from the hole center. It is observed in all of irradiated silica glasses below 60 K. The T_p times for this center are comparable to those for the hole centers, while its T_s times are 3–4 times shorter. In some samples, the $g_{\text{eff}} \sim 2$–2.21 signal overlapped with an equally weak resonance signal from a center with g_{eff} between 2 and 2.6. The broader EPR signal is from Cu^{II} impurity centers. In glasses made with suprasil II, this center is absent, and the $g_{\text{eff}} \sim 2$–2.21 center can be observed without interference.

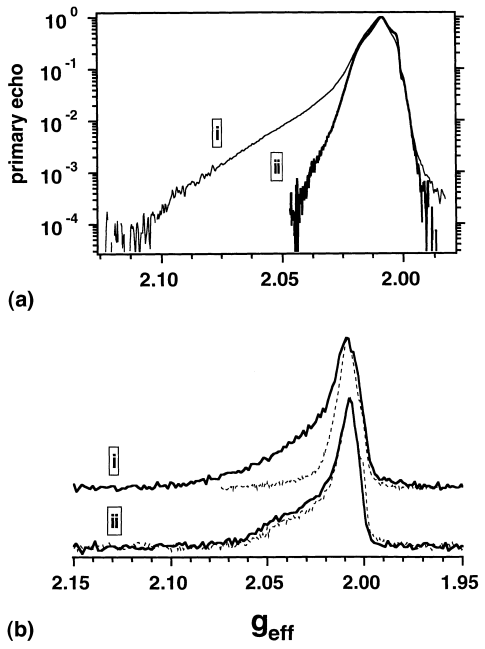

Fig. 8. (a) Field-swept pESE spectra from irradiated K-3 glass. The spectra were obtained at 14 K (i) and 100 K (ii), respectively. Notice the log scale for echo signals. The 'tail' between $g \approx 2$ and $g \approx 2.15$ is from Si peroxy radicals. At 100 K, only signals from the hole and E′ centers were observed. (b) pESE spectra from Na-3 class doped with 0.6 wt% of Ce^{III}. In this glass, the yield of OHC decreases 15-fold, and the signal from peroxy radicals is clearly discernible. Bold traces were obtained at 12 K, dashed traces at 56 K; traces (i) are for the sample irradiated to 2.3 MGy at 300 K, traces (ii) – for the same sample annealed at 600 K for 1 min. The traces were normalized at $g_{\text{eff}} \approx 2.01$ (the echo signals from OHC at 56 K are 10 times weaker than the signal from peroxy radicals at 12 K). Annealing at 600 K reduces the intensity of the pESE signals by an order of magnitude and completely removes the signals from OHC; the signal from peroxy/superoxide radical is still there.

The line shape of the $g_{\text{eff}} \sim 2$–2.21 signal and its relaxation and annealing behavior are similar to those for silicon peroxy radical in fused silica. Both these signals are unobservable with ESE above 60 K (unfrozen tumbling motion of the peroxy group causes rapid T_2 relaxation); their relaxation times are similar. In alkali silicates, the $g_{\text{eff}} \sim 2$–2.21 signal persisted after thermal annealing at 600–650 K (Fig. 8(b)). From cw EPR studies of Cases and Griscom [71], it is known that

this treatment removes the signals from oxygen hole and E′ centers leaving weaker EPR signals from peroxy radicals. On the basis of these observations, we concluded that the $g_{\rm eff} \sim 2$–2.21 signal is from silicon peroxy radical.

The radiolytic yield of peroxy radical remains roughly the same when the glass is irradiated at 77 and 300 K. While doping of Na and K glasses with Ce^{III} removes most of the EPR signal from the hole centers, it has little effect on the yield of peroxy radicals (Fig. 8(b)); the same applies to doping the glass with electron scavengers, such as Ti^{IV}. Thus, the peroxy radical is neither the electron nor the hole center. Its formation is not thermally activated and is likely to proceed through the decay of self-trapped excitons (relaxed L-centers?), as in fused silica. The dose dependence of the EPR signal from the peroxy radical parallels that for the E′ center and is different from that for oxygen hole centers. This suggests that silicon peroxy and dangling bond centers are formed in the same radiolytic reaction.

4.4. Cesium glasses

Good-quality ESE data for cesium glasses (Cs-3) can be obtained only below 60 K; at higher temperature, the phase relaxation is too fast. The ESE signal is spread over 15 mT (with $g_{\rm eff}$ between 1.96 and 2.06) and centered at $g_{\rm eff} \approx 2.01$ (Fig. 9(a)). This broad signal overlaps with the signal from E′ center and a weak signal from Ti^{III} center. Similar EPR signal in cesium glasses was observed in Ref. [75]. A remarkable feature of this signal is that there is no change of the ESEEM pattern across its entire span (except for the small change in the NMR frequency), cf. Fig. 9(b). This suggests that the signal is from a *single* species. The spin–lattice relaxation times for this center are field-dependent: for $g_{\rm eff} > 2.01$, $T_{\rm s} \approx 0.16$ ms, for $g_{\rm eff} < 2.01$ the $T_{\rm s}$ time systematically shortens with $g_{\rm eff}$. In the high-field wing, the relaxation times are quite long: e.g., for $g_{\rm eff} = 1.98$, $T_{\rm s} = 0.26$ ms (12 K). This range of $T_{\rm s}$ times is typical for OHC_1 (see above). The same broad EPR line was observed with cw EPR to 450 K; at higher temperatures the hole center anneals. Doping the glass with Ce^{III} removes this signal from EPR spectra. These observations suggest that *the broad EPR signal is from the cesium variant of* OHC_1. Unlike the EPR line for OHC_1 in K glasses, this signal extends well below $g_{\rm e}$. To a lesser degree, the EPR lines of OHC_1 in Li and Na glass also exhibit such extensions. We repeat that this widening is a result of *inhomogeneous* broadening. Apparently, all three components of the g-tensor were perturbed by the crystal field of the cation. *There is no special arrangement for the O 2p orbital relative to the Alk–NBO–Si plane.*

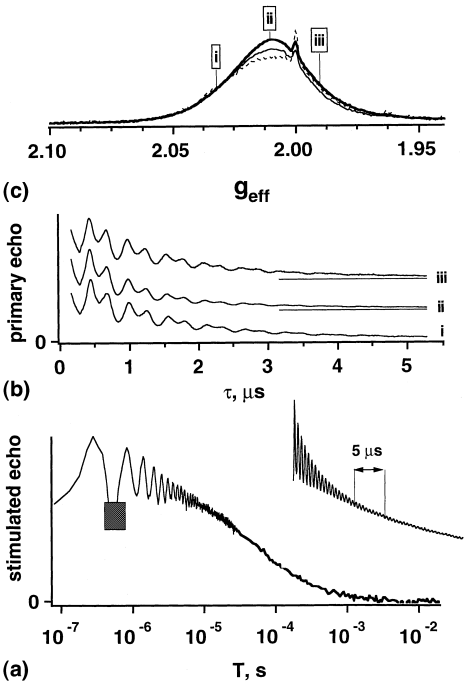

Fig. 9. (a) Field-swept pESE spectra from Cs-3 glass irradiated to 1 MGy at 300 K. The spectra were obtained at 12 K using 70 ns excitation pulse. The signal at $g_{\rm eff} \approx 2$ is from E′ center; the signal with $g_{\rm eff}$ between 1.95 and 2.1 is from OHC (a weak signal from Ti^{III} at $g_{\rm eff} \approx 1.97$ from is swamped by this broad signal). (b) Primary ESE kinetics for spin packets (i)–(iii) marked in (a). The modulation is due to spin coupling to ^{133}Cs nuclei in the sample. Note how little the pattern changes between the field positions. (b) Stimulated ESE kinetics for spin packet (ii) (20 ns pulse, repetition rate 50 Hz) obtained for optimum $\tau = 0.28$ μs ($\approx 0.5\nu_{\rm I}^{-1}$). The 'blind spot' at $T = 2\tau$ is shaded. Pay attention to the log scale for delay times T. The initial part of the sESE kinetics ($T < 20$ μs) is shown separately on the proportional timescale.

The E′ center in cesium trisilicate glass has relaxation times and spin parameters that are closer to those for E'_γ center in fused silica than to the E′ centers in K and Na glasses: Compare T_p of 1–2 μs in K-3 and Na-3 glasses with $T_p = 85$ μs in Cs-3 glass (at 300 K). The field-swept pESE spectrum of the E′ centers in Cs-3 is indistinguishable from that for E'_γ center in silica. There could be only one conclusion: the E′ centers in Cs-3 glass are formed in Si-rich domains. This glass is microscopically phase-separated.

4.5. ESEEM in hole centers

While the spin centers in ^{39}K silicate glasses exhibit no echo modulation, the spin centers in ^{23}Na, ^{133}Cs, and ^{7}Li glasses all demonstrate modulation by the alkali nuclei (Figs. 9–12). The stimulated (s)ESEEM is easier to interpret since the envelope is modulated at a single frequency. Fig. 9(c) demonstrates sESE kinetics for OHC_1 in low-temperature Cs-3 glass; its Fourier transform (FT) spectrum is shown in Fig. 10(a), trace (i). These sESE kinetics were obtained for optimum $\tau \approx 1/2\nu_I$, where ν_I is at the NMR frequency of the alkali nucleus. The sESEEM spectrum shown in Fig. 10(a) consists of a single narrow line centered at ν_I for ^{133}Cs. There is no discernible quadrupolar structure. The linewidth of the FT sESEEM signal correlates with the quadrupolar moment of the alkali nucleus: for OHC_1 in Cs-3 and Na-3 glasses, the line widths are 90 and 450 kHz fwhm, respectively (cosine FT; Fig. 12, trace (i)).

Since the modulation pattern is simple and the nuclei are weakly coupled, the average distance between the nuclei and the spin center can be estimated from the modulation depth λ [8]

$$\lambda = 1 - E_{\min}/E_{\max} = 16/5I(I+1)[g_e\beta_e/B_0]^2\bar{r}^{-6}, \quad (3)$$

where I is the nuclear spin and $\bar{r}$ is the average distance to the weakly coupled nuclei, $\bar{r}^{-6} = \sum_j r_j^{-6}$. For Na-3 and Cs-3 glasses, the estimates for $\bar{r}$ are 0.32 and 0.42 nm, respectively. These distances change little with the molar fraction of alkali modifier. For example, in Na-19 glass, the distance $\bar{r}$ is only 5% longer than in Na-3 glass. This suggests that the contribution from the nearest alkali cations is predominant. The distances $\bar{r}$ determined from sESEEM correlate with typical Alk–NBO distances elucidated from MD analyses [13–21] and EXAFS and XANES studies [10]. Interestingly, these distances better correspond to the first peaks in the Alk–Alk distribution than the first peaks in the Alk–NBO distribution. Either the alkali cation that compensates NBO is missing in the hole center, or its signal is missing from the sESEEM spectra.

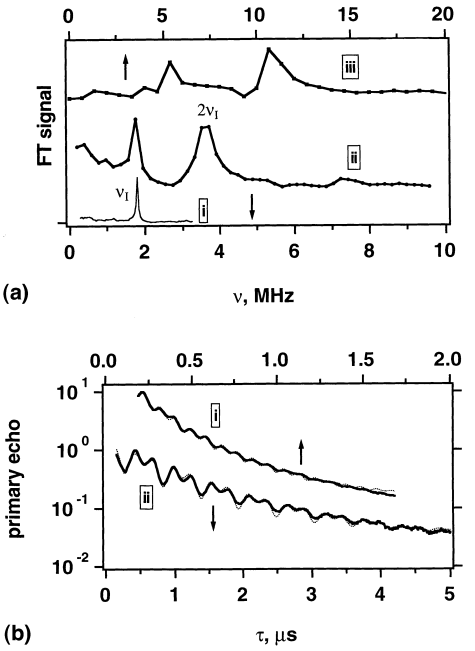

Fig. 10. (a) Power FT spectra for OHC in Cs-3 ((i) and (ii)) and Li-3 (iii) glass at 12 and 20 K, respectively. Bold traces (ii) and (iii) are primary ESEEM spectra, trace (i) is stimulated ESEEM spectrum for $\tau = 0.28$ μs. The kinetics were obtained with 20 ns excitation pulse. In primary ESEEM spectra, resonances at ν_I and $2\nu_I$ for ^{133}Cs are indicated with symbols. The arrows indicate the frequency scale for the corresponding traces. (b) Fitting primary ESE kinetics for OHC in Li-3 (i) and Cs-3 (ii) glasses using Eq. (5).

For weakly coupled nuclei, the modulation kinetics of primary echo is given by Dikanov and Tsvetkov [8]:

$$E(\tau) = 1 - \lambda/8\{3 - 4\cos(\omega_I\tau) + \cos(2\omega_I\tau)\}, \quad (4)$$

where λ is given by Eq. (3), and $\omega_I = 2\pi\nu_I$. The corresponding power FT spectrum consists of two

components at ν_I and $2\nu_I$ with the ratio ζ between their amplitudes equal to 4:1. The FT spectra for OHC_1 in ^{133}Cs, ^{7}Li and OHC_2 in ^{23}Na glasses exhibit the same oddity: the pESE kinetics are indeed modulated at ν_I and $2\nu_I$, as expected for weakly coupled nuclei, but the ratio ζ is between 0.2:1 and 2:1 (Figs. 10–13). This is not a result of some error: in Na-1.3 glass, the Ti^{III} center has pESEEM spectrum that shows approximate 4:1 ratio between the components while the OHC_2 has spectrum with 1.5:1 ratio between the same components (Fig. 11(a)). The sESEEM spectra from these centers did not indicate strong quadrupolar broadening (the width of the lines in pESEEM spectra are limited by the length of the sampling window determined by the T_p time).

We found that the pESE kinetics can be simulated using a generalized form of Eq. (3)

$$E(\tau) = E_0(\tau)\{1 + A_1\cos(\omega_I\tau)\exp[-\gamma_1 t] - A_2\cos(2\omega_I\tau)\exp[-\gamma_2 t]\}, \quad (5)$$

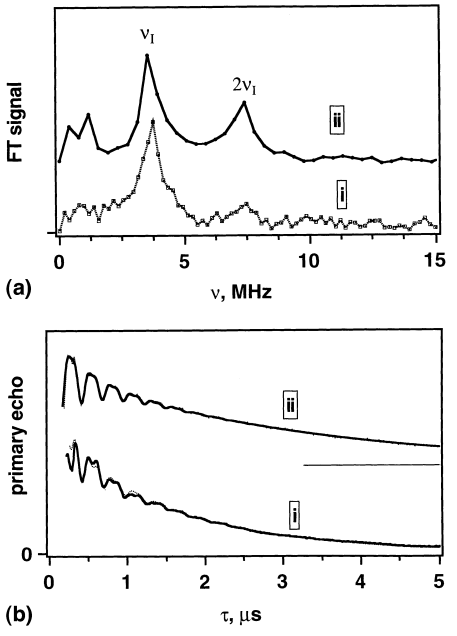

Fig. 11. (a) Power FT pESEEM spectra for Ti^{III} center (i) and OHC_2 (ii) in Na-1.3 glass irradiated to 1 MGy at 300 K. The ESE kinetics were obtained at 12 K. The pESE kinetics were obtained with 20 ns μw excitation pulse. The resonances at ν_I and $2\nu_I$ for ^{23}Na are indicated with symbols. (b) Fitting primary ESE kinetics for OHC_2 (i) and Ti^{III} (ii) using Eq. (5).

where $A_1,\ A_2 > 0$ and $E_0(\tau)$ is the decay kinetics of spin echo in the absence of modulation (which was simulated with a stretched exponential or biexponential dependence). According to Eq. (5), the ratio ζ of the ν_I and $2\nu_I$ components in the power FT spectrum is $(A_1/\gamma_1^2):(A_2/\gamma_2^2)$. For ^{133}Cs and ^{7}Li centers (traces (ii) and (i) in Fig. 11(b)), we let $\gamma_1 \approx \gamma_2 \approx 0$ and obtained ζ of 1.1 and 0.3:1, respectively. For Ti^{III} and OHC_2 in Na-1.3 glass, the fitting procedure gave the $A_1{:}A_2$ ratio of 4.4:1 and 1:1 and $\gamma_1{:}\gamma_2$ ratio of 0.8:1 and 1.8:1, respectively (Fig. 11(b)). For OHC_1 in Na-3 and Na-19 glasses (Figs. 12 and 13), good fits of pESE kinetics can be obtained only when either the coefficient A_1 is small or the line width γ_1 is several MHz. Indeed, in the power FT ESEEM spectra of these centers, the $\nu = \nu_I$ component is either reduced or spit into two halves, depending on the sample temperature (Fig. 12). This behavior will be examined in Section 5.

Since the ESE signal from E′ centers overlaps with the signal from hole centers, its modulation pattern cannot be studied.

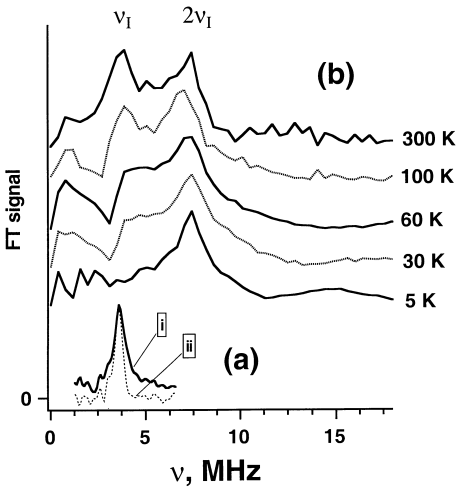

Fig. 12. Stimulated (a) and primary (b) FT ESEEM spectra for OHC_1 in irradiated Na-3 glass. The stimulated ESE kinetics were obtained at 12 K with $\tau = 0.15$ μs. Power FT (i) and cosine FT sESEEM spectra (ii) are shown in (a) with bold and dashed lines, respectively (no apodization was used). Traces (b) are FT pESEEM spectra obtained between 5 and 300 K. Note the systematic increase in the FT pESEEM signal at $\nu \approx \nu_I$ (3.6–3.7 MHz) relative to the signal at $\nu \approx 2\nu_I$ with the temperature.

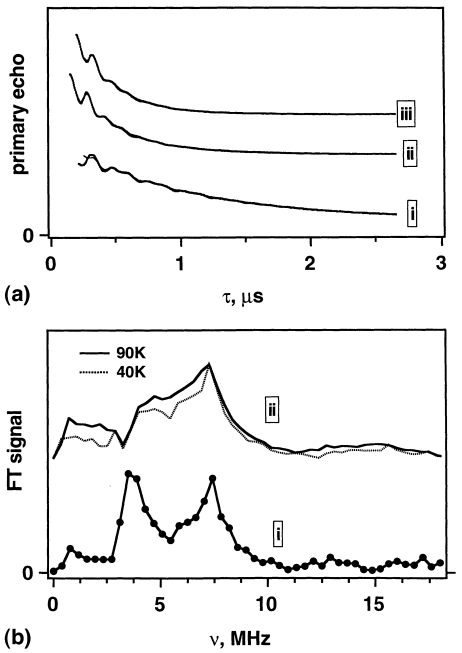

Fig. 13. (a) Primary ESE kinetics for OHC_1 in Na-19 glass irradiated to 10 kGy (traces (i)) and 1 MGy (traces (ii) and (iii)) at 300 K. The ESE kinetics were obtained at 40 K ((i) and (ii)) and 90 K (iii), respectively. Dots are experimental traces, lines – simulations obtained using Eq. (5). (b) Power FT spectra for traces shown in Fig. 13(a).

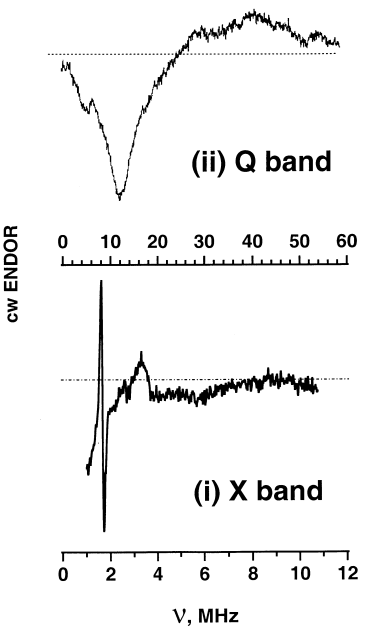

Fig. 14. X-band (i) and Q-band (ii) continuous-wave ENDOR spectrum from OHC_1 in Cs-3 glass. The narrow line at $\nu \approx \nu_I$ is from weakly coupled $^{133}Cs^+$ cations; the broad line at 3–4 MHz in trace (i) is either from strongly coupled $^{133}Cs^+$ cations or a forbidden $\Delta M = \pm 2$ transition.

4.6. Continuous-wave ENDOR for OHC_1

Since the X band ENDOR spectrometer operated at radio frequencies above 1 MHz, we were not able to observe the ENDOR signals from ^{39}K. The μw pumping was carried out at the maximum of the EPR signal, at $g \approx 2.01$. ^{133}Cs and ^{7}Li glasses both showed an ENDOR signal at $\nu \approx \nu_I$ from weakly coupled (matrix) alkali cations; only in ^{133}Cs glasses an additional broad signal at 3–4 MHz was observed (Fig. 14). These ENDOR signals were very weak; ca 1 h averaging was required to obtain signal-to-noise ratio of 10. No ENDOR from ^{23}Na glasses was observed. This is due to poor μw saturation of hole centers in Na glasses and relatively large quadrupole moment for ^{23}Na nuclei.

The frequency of the 3–4 MHz signal in Cs-3 glass is close to $2\nu_I$ (calculated $\nu_I \approx 1.87$ MHz; the narrow signal is at 1.65 MHz). This resonance signal could be from a forbidden NMR transition. However, the 3–4 MHz signal (at 15% of the $\nu \approx \nu_I$ signal) seems to be too strong for a $\Delta M = \pm 2$ transition, and the quadrupole moment for ^{133}Cs is too low to account for the violation of selection rules (see Fig. 10(a)). It is possible that the broad ENDOR signal is from the $\pm 1/2 \rightarrow \pm 3/2$ transition in ^{133}Cs with $a_{iso} \approx 3.8 \pm 0.5$ MHz ($\nu = |\nu_I \pm a_{iso}/2|$). The broadening of the ENDOR line could be indicative of a wide distribution of a_{iso}. Using the atomic hyperfine coupling constant of 2.3 GHz [9], we estimate that the spin density on the Cs 6s orbital would be $(4–5) \times 10^{-2}$. The Q-band (35 GHz) ENDOR spectrum of the same Cs-3 sample exhibits a broad line centered at 13.6 MHz which corresponds to $\nu \approx 2\nu_I$ and a much weaker $\nu \approx \nu_I$ line at 7 MHz. The comparison between the X- and Q-band ENDOR spectra suggests that the 3–4 MHz feature in Fig. 14 is likely to be from the forbidden NMR transition. There is no evidence for strongly coupled ^{133}Cs nuclei with well-defined a_{iso}.

4.7. Peroxide/superoxide radicals

For peroxy/superoxide radicals in Na silicate glasses, the spin echo envelopes are strongly modulated by ^{23}Na. Due to the small amplitude of the echo signal and fast T_2 relaxation in this center, the FT analysis is not feasible. Nevertheless, it is clear that *the peroxy/superoxide radicals involve alkali cations more strongly than the hole centers.* For example, the $g_{\text{eff}} \sim 2.01$ signal in trace (ii), Fig. 8(b) exhibits the modulation depth $\lambda \approx 0.45$, while for OHC_1 in the same glass, $\lambda \approx 0.2$. The exact way in which ^{23}Na nuclei are coupled to the radical cannot be presently determined.

Cases and Griscom [71] found that annealing at 580 K removes peroxy radicals leaving interstitial $O_2{\cdot}^-$ anions. The latter species has axial g-tensor with $g_\perp \approx 2$ and $g_\parallel$ around 2.14. Whether before or after the annealing, *such resonance signal was not observed in field-swept pESE spectra*, though there were small changes in the broad line of peroxy radicals for $g_{\text{eff}} > 2.06$. It is conceivable that the sensitivity of echo detection is insufficient to observe the $g_{\text{eff}} \approx g_\parallel$ signal from $O_2{\cdot}^-$ (this is possible if the T_2 time at 4 K is very short). Field-modulation cw EPR is more sensitive to small changes in line shapes and allows to detect centers with short T_2 times. Therefore, we tried to reproduce the result of Cases and Griscom [71] using cw EPR. Though considerable evolution in the wings of cw EPR signal from peroxy radical was found, these changes varied from glass to glass, from sample to sample, and were different for samples with different irradiation and thermal history. In no instance did we observe the changes reported in Ref. [71]. We have no explanation for this discrepancy.

On the other hand, data on ESEEM and spin relaxation in the peroxy/superoxide radical are consistent with observations of Cases and Griscom [71]. Annealing at 580 K twice reduces the T_p time for this radical. At the same time, the modulation depth λ of the ESEEM increases from 0.35 to 0.45 indicating stronger coupling to ^{23}Na cations (in $Na_2O \cdot 3SiO_2$ glass). Faster O–O tumbling and stronger coupling to alkali cations is expected for an interstitial anion. However, the same changes can be explained by thermally activated migration of alkali cations. The cation may couple to the terminal oxygen of Si peroxy radical, weakening the Si–O bond and making the tumbling of the O–O fragment faster. Precisely that was revealed in our simulations.

We believe that the 'silicon peroxy radical' is, actually, a class of $\equiv SiOO{\cdot}Alk^+$ defects with variable Si–O and O–Alk separations. The existence of such an ensemble explains remarkable variability of cw EPR spectra with the thermal history of the sample. Whether or not the interstitial $O_2{\cdot}^-$ is formed in irradiated alkali silicate glass, its generation *requires* high-temperature annealing.

4.8. OHC in 'wet' silica

It has been speculated that OHC in 'wet' silica is an OHC_1-like defect **I** in which the alkali cation is replaced with a proton [68]. Since both H and D nuclei are magnetic, we tried to observe ESEEM from oxygen hole centers in OH and OD 'wet' silica (Suprasil II). The H/D exchange was carried out as described in Ref. [102]. Since the concentration of siloxyl groups is ~0.1 wt% the modulation of spin echo by 'distant' OH groups is negligible.

We found no modulation of spin echo envelope from OHC by H and D nuclei. It appears that the OHC in 'wet' silica is not (even weakly!) coupled to a hydroxyl proton. The only other possibility is that this proton is coupled very strongly ($a_{\text{iso}} > 0.5$ mT), but not strongly enough for the hyperfine structure to be resolved by cw EPR. This is very unlikely, since the modulation pattern was also lacking in the OD-substituted silica. It appears that *the OHC in 'wet' silica does not involve a nearby siloxyl group.* Our unexpected result suggests that an ENDOR study must be carried out to verify this conclusion.

4.9. Electron centers

Intrinsic spin-1/2 electron centers were sought for using pulsed and cw EPR. K and Na silicate

glasses were irradiated at 77 K using 3 MeV electrons or 30–120 mJ pulses from an excimer laser operating at 248 or 308 nm. Some glasses were ionized with 308 nm laser pulses at 4 K, in situ. Electrons were injected by laser excitation of cations in photochromic glasses (such as Ce^{III} doped glass). In all these experiments, *no intrinsic electron centers were observed by EPR*.

Next we tried to observe these centers with pulsed ODMR in the 9 GHz band. At 10–300 K, the Boltzmann polarization is small, and ODMR can be observed only from spin-correlated electron–hole pairs. Initially, these pairs have singlet correlation; later they become triplet correlated due to faster recombination of singlet pairs [60]. ODMR critically depends on the rates of T_1 and T_2 relaxation in the pair: if the spin relaxation is fast, the spin correlation is destroyed faster than generated, and the ODMR is not observed.

The electron–hole pairs were generated using a 5-to-50 ns pulse of 3 MeV electrons. The photoluminescence (PL) of the L-centers in $Na_2O \cdot 3SiO_2$ glass was observed at 3.5 eV. Three time-resolved ODMR experiments were carried out: (i) a short 0.02–4 μs, 0.5 kW microwave pulse was applied 10^{-8}–10^{-5} s after the electron beam pulse and the PL was detected right after this excitation μw pulse [103]; (ii) a long (10–100 μs) 1 mW pulse was applied for every second electron beam pulse and a lock-in amplifier was used to observe μw-induced change in the PL on the millisecond timescale; (iii) the electron beam was run continuously, the 1 mW microwave pulse turned on and off for half-period (10–500 μs), and the lock-in amplifier used to detect variation in the PL [104]. No ODMR was found in all three of these experiments.

We conclude that above 10 K, electron centers are either diamagnetic or have very short T_2 times ($<10^{-8}$ s). [2]

[2] Our results do not contradict the ODMR study of Baker et al. [60]. These workers continuously pumped μw transitions for a pair with large Boltzmann polarization. Thus, even the species with short relaxation times were detected. This approach cannot be implemented for prompt PL at higher

5. Discussion

5.1. Asymmetric T_2 relaxation in OHC_1

Phase relaxation observed for OHC_1 in K and Na silicate glasses (above 170 and 80 K, respectively) is strongly asymmetric: phase memory times for centers with $g_{\rm eff} < g_2$ are longer than for centers with $g_{\rm eff} > g_2$. For centers whose resonance fields $B_{\rm res}$ are in the low-field wing of the EPR spectrum, $T_{\rm p}$ times are independent of $g_{\rm eff}$.

For OHC_1 in K-5 glass, the cw EPR spectrum was accounted for in terms of a radical with g-tensor whose principal $\{g_k\}$ values are distributed according to Eq. (1) [68]. The only reasonable source of *asymmetric* T_2 relaxation is the perturbation of the g-tensor by a low-amplitude atomic motion. Indeed, other sources of phase relaxation do not account for the observed features: Dipolar relaxation results in a different relaxation pattern (cf. Fig. 2(a) and (b)). ^{39}K nuclei have too small dipole and quadrupole moments to cause spin relaxation in the studied temperature range.

Asymmetric T_2 relaxation due to modulation of g-tensor through orbital perturbation was previously studied for radicals in organic glasses [105]. Consider a spin center with a molecular-frame g-tensor $\{g_i\} = (g_{xx}, g_{yy}, g_{zz})$, and let $\Omega = (\theta, \phi)$ be the Euler angles. For $\Delta g_i \ll g_{\rm e}$,

$$g_{\rm eff}(\Omega) \approx g_1 \sin^2\theta\cos^2\phi + g_2 \sin^2\theta\sin^2\phi + g_3\cos^2\theta. \tag{6}$$

The T_2 time for the corresponding spin packet is given by

$$T_2^{-1}(\Omega) = 1/4\,\omega^2\tau_{\rm c}\langle\{g_{\rm eff}(\Omega) - \langle g_{\rm eff}(\Omega)\rangle\}^2\rangle, \tag{7}$$

where $\tau_{\rm c}$ is the correlation time of the tumbling motion and $\langle\cdot\rangle$ means averaging over non-spin variables. Griscom [68] found that the distribution of $\{g_i\}$ values for OHC_1 in K glasses can be explained through a distribution of a single parameter, the orbital energy Δ (Eq. (1)). Let us first assume that g_k varies through the variation in Δ, so that $g_k - \langle g_k\rangle \approx \langle g_k - g_{\rm e}\rangle\delta\Delta/\Delta$. In this case, combining Eqs. (6) and (7) we obtain

$$T_2^{-1}(\Omega) \propto \langle\{\delta\Delta/\Delta\}^2\rangle\langle g_{\rm eff}(\Omega) - g_{\rm e}\rangle^2. \quad (8)$$

According to Eq. (8), T_2^{-1} increases as $|g_{\rm eff} - g_e|^2$. A systematic increase of $T_{\rm p}$ with $|g_{\rm eff} - g_e|$ was indeed observed for OHC_1 (Fig. 2(a)). However, Eq. (8) does not explain why the $T_{\rm p}$ times were independent of $g_{\rm eff}$ for resonances with $g_{\rm eff} \approx g_3$. Apparently, the orbital perturbation of the g-tensor cannot be reduced to changes in Δ. Let us assume that only one component of the g-tensor varies, g_3. Then

$$T_2^{-1}(\theta) \propto \langle\{g_3 - \langle g_3\rangle\}^2\rangle \cos^4\theta. \quad (9)$$

Formula (9) indicates that the fastest T_2 relaxation will occur for resonances with $\theta \approx 90°$, i.e., $g_{\rm eff} \approx g_3$. As the angle θ departs from 90°, the decrease in T_2^{-1} is steep. At the centroids of g_1 and g_2 resonances ($\theta \approx 0°$) the T_2 relaxation is slow. Since the $\{g_k\}$ values are distributed over a wide range, for a given resonance field $B_{\rm res}$ many centers with different Euler angles Ω contribute to the EPR signal, and the observed T_2 time is a dynamic average over this set. These Ω sets can be found using distributions for $\{g_k\}$ given by Griscom [68]. Analysis of these sets for different $g_{\rm eff}$ indicates that in the low-field wing of the EPR spectrum, 70-to-100% of the resonance signal is from spin centers with $\theta \sim 80$–$90°$. This is understandable: in the low-field wing, there are fewer centers for which $\theta \ll 90°$ and $g_3 > g_{\rm eff}$. For this reason, the rate of the T_2 relaxation varies little over the high-$g_{\rm eff}$ region where most centers have $\theta \approx 90°$. Our calculations suggest that in order to confine the T_2 relaxation to the low-θ region, the orbital perturbation of the g-tensor must be confined to the z-axis of the molecular frame.

We conclude that the observed behavior may be explained through perturbation of the g_{zz} component by a low-amplitude fast atomic motion. Since the z-axis is the direction of the Si–NBO bond and the temperature at which the motion is activated correlates with alkali cation size, it is reasonable to assume that the g-tensor is modulated by rocking motion of the cation in the immediate vicinity of the OHC_1. This motion modulates the crystal field of the cation at the spin center, perturbing its g-tensor.

5.2. ESEEM

Why is the ζ ratio for Ti^{III} center equals the theoretical value of 4:1 whereas for hole centers it is considerably lower? The obvious difference between the oxygen hole center and the Ti^{III} center is their coupling to alkali cations. While the hole center may or may not be strongly coupled to alkali cations, the Ti^{III} center is a trigonally distorted, octahedrally coordinated cation shielded from the alkali cations by ligand oxygens [57,58]. Kordas [82] has studied pESE kinetics for OHC_1 in Li-10 glass and obtained a modulation pattern very similar to that shown in Fig. 10(b) for OHC_1 in Li-3 glass. This pattern was simulated using Eq. (5) for weakly coupled nuclei (the kinetics were averaged over NMR frequencies that had Gaussian distribution centered at $\nu_{\rm I}$). It is simple to demonstrate (see Chapter 6, part IV in Ref. [8]) that as a result of such averaging, the ratio ζ is even greater than 4:1 since it predicts $\gamma_2 \approx 2\gamma_1$ (Eq. (5)). Therefore, it is not surprising that the quality of the fit in Ref. [82] was poor.

We have made numerous calculations of ESEEM kinetics in order to determine how such factors as quadrupolar coupling and space distribution of spin-3/2 nuclei can reduce the 4:1 ratio. We also studied how partial excitation of the spectrum with finite-duration μw pulse may change this ratio. We found that none of these factors can account for the observed ESEEM pattern.

Recently, Kordas and co-workers [83] revisited the same system and studied OHC_1 in Li glass using a 2D pulsed EPR spectroscopy and found a subset of Li nuclei that were strongly coupled to OHC_1 with isotropic hyperfine coupling constant $a_{\rm iso} \approx 0.5$ MHz and $T_\perp \approx 4$ MHz (in the point dipole approximation, $T_\perp = g_{\rm e}\beta_{\rm e}g_I\beta_I r^{-3}$, where r is the electron–nuclear distance). We have tried to simulate our pESEEM kinetics using these values for $a_{\rm iso}$ and $T_\perp$, but the fit was still poor.

The FT pESEEM spectra with reduced ζ have been observed in other ESEEM studies [8]. The reduction was explained trough a wide distribution of a_{iso} for strongly coupled nuclei. For non-zero a_{iso}, each $\nu = \nu_I$ resonance signal in the FT spectrum is split into two signals (ν_α and ν_β) with $|\nu_\alpha - \nu_\beta| \sim a_{iso}$. At the same time, the amplitude $2\nu_I$ is not changed since $\nu_\alpha + \nu_\beta \approx 2\nu_I$. If a_{iso} are distributed over some range, the $\nu_{\alpha,\beta}$ lines would sum up to give a structureless broad signal that would be filtered out by the FT procedure. Then, the signal at $\nu = \nu_I$ would come mainly from weakly coupled distant nuclei for which $a_{iso} \approx 0$.

This picture qualitatively explains the observed features: (i) the prominence of weakly coupled nuclei in sESEEM, (ii) the reduced ratio ζ between the ν_I and $2\nu_I$ components in the FT pESEEM spectra from Cs and Li silicate glasses, (iii) considerable broadening and overlap of the ν_I and $2\nu_I$ signals for Na silicate glasses (see below). Furthermore, this picture is consistent with the HYSCORE results of Kordas and coworkers [83,84]: it is conceivable, that in a subset of hole centers with non-zero a_{iso}, some cross-peaks in the HYSCORE spectra are particularly well resolved.

Unfortunately, our model is difficult to implement numerically, as one needs to know how a_{iso} varies as a function of r. The following approach was used: The isotropic hyperfine constant was varied as $a^0_{iso}\exp(-\alpha[r - r_m])$, where $\alpha \approx 0.2$ nm^{-1} and r_m is the minimum Alk–OHC approach. The Alk–NBO distribution $\rho(r)$ given by MD calculations in Refs. [13–18] was used for r, and the ESEEM patterns were weighted by $r^2\rho(r)$. We assumed that the angular distribution of cations was random. Using $a^0_{iso} \approx 10$–30 MHz, we obtained FT pESEEM spectra that much resembled the experimental ones. These simulations showed that the deviation from the 4:1 ratio is stronger for stronger coupled alkali nuclei. This suggests that in OHC_2, where ζ is close to 2:1, the alkali nuclei are less coupled to the spin center than in OHC_1, for which ζ varies from 0.5:1 to 1:1.

In Na-3 glasses, the pESEEM spectra are temperature-dependent. At low temperature, the ν_I line is split in two components separated by 2–3 MHz (corresponding to $a_{iso} \approx 1$–1.5 MHz); as the temperature increases, the ν_α and ν_β subcomponents collapse into a single line at $\nu \approx \nu_I$ (with ζ approaching 1:1 at 300 K). The same 1:1 spectrum can be observed, with better resolution, in Na-19 glass irradiated to a lower dose (Fig. 13(b)). When the dose is increased, the pESEEM spectra look like those in Na-3 (Fig. 12, (ii)). Apparently, in Na glasses there is a subset of hole centers that are coupled to a ^{23}Na cation with a_{iso} of 1–1.5 MHz (Astrakas and Kordas gave the estimate of $a_{iso} \approx 1 \pm 0.1$ MHz and quadrupolecoupling constant of 1 ± 0.4 MHz [84]). As the temperature increases, the nucleus starts to swing and a_{iso} averages out to lower values. Remarkably, the onset for the $\nu \approx \nu_I$ line is at 80–100 K, the same temperature at which the T_2 relaxation in Na-3 becomes asymmetric (see above). *The correlation between these two changes suggests that the motion activated at higher temperatures is that of a neighboring alkali nucleus.*

5.3. Modeling the centers

The radiation-induced centers were modeled using semi-empirical MNDO (or MNDO/d) and ab initio UHF/STO-3G methods (programs from the SPARTAN package). Since MNDO supports no alkali nuclei other than Li, only lithium centers were modeled in this work. Following the usual protocol (e.g., Refs. [106,107]), some BOs were replaced with hydrogen-terminated NBOs to reduce the cluster size. Since Li^+ is fourfold coordinated in lithium silicate glasses [10], in some MNDO calculations three H_2O molecules were arranged around the cation in such a way this cation was at the center of a tetrahedral complex. If not stated otherwise, the numbers given below refer to the MNDO calculations.

5.4. OHC_1

Three types of $\equiv$SiO$\cdot$ structures were used to model OHC_1: $(HO)_3SiO\cdot$ (**V**), $(HO)_3SiO\cdot\ Li^+$ (**VI**) and $\{(OH)_3SiO\}_3SiO\cdot\ Li^+(OH_2)_3$ (**VII**).

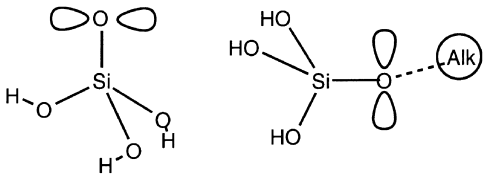

V VI

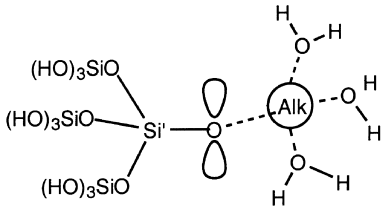

VII

Structure **V** is a cation-stripped variant of the OHC_1, and its electronic structure agrees well with the model given by Griscom [68]: the spin density is mainly on NBO 2p orbital, with small spin density on silicon. Structure **VI** is a hole on the NBO–Li^+ unit; its ground state corresponds to the precursor of OHC_1 and the L-center. In the precursor, the O–Li bond is ionic (the charge on NBO and Li is -1.28 and $+0.74$, respectively; r(NBO–Li) = 0.167 nm and r(NBO–Si) = 0.165 nm). After geometry optimization, both the MNDO and ab initio calculations yield the Si–NBO–Li angle close to 180° (this angle reduces to 108° in an analogous Na^+ center). When the water cage for Li^+ is included to simulate the effect of BOs (**VII**), the Si′–NBO–Li angle changes to 170°, the charge on Li reduces to +0.51, r(NBO–Li) increases to 0.185 nm, while $r(H_2O–Li) = 0.22$ nm. These bond lengths compare well with the maxima in the O–Li distribution obtained in MD simulations. It seems, however, that MNDO overestimates the ionic character of the O–Li bond. The ab initio calculation gives lower charges on NBO and Li in structures **V** and **VI** (-1.1 and +0.55, respectively, r(Li–NBO) = 0.17 nm). No significant changes between the structures with C_{3v} symmetry and C_1 symmetry was found.

Upon ionization of the neutral species, almost all the spin density resides at the NBO. A geometry optimization yields clusters with elongated Li–NBO and Si–NBO bonds. In structures **VI** and **VII**, the Li–NBO bond elongates to 0.20 and 0.21 nm, respectively, while the Si–NBO bond elongates to 0.172 nm. Without the water cage, the charge on Li increases to +0.94 and the charge on NBO decreases to -0.6; the spin density on Li is 6×10^{-3} and the spin density on Si is 0.042. In **VII**, the charge on Li cation reduces to +0.41 since the positive charge is shared by the BOs, and the spin density on Li increases to 0.012. Both the spin density and the Li–NBO distance for **VII** are close to the ones determined by Kordas and co-workers [83]. We were, however, unable to reproduce the Si–NBO–Li angle of 120° reported by these workers. The error may lie with the experiment rather than our calculations, since HYSCORE is not very sensitive to the *angular* distribution of nuclei.

For OHC_1 in K glasses, g_{xx} component of the g-tensor is narrowly distributed around g_e suggesting that the crystal field has planar symmetry. Griscom [68] accounted for this observation assuming that the O 2p orbital is perpendicular to the Si–NBO–Alk plane. In other alkali silicate glasses (in particular, Cs silicate glasses), there is a considerable extension of the EPR spectrum to lower g_{eff}. This suggests that the planar symmetry of the crystal field is broken. To study this effect, we performed an ab initio calculation for neutral $(HO)_3SiOAlk$ species, optimized their geometry, and determined the angle between the NBO 2p orbital in the HOMO and the Si–NBO–Alk plane. For Li^+ and Rb^+, these angles are 90° and 20°, respectively: When the alkali cation is large, its interaction with BOs reduces the Alk–NBO–Si angle. For Li^+ and Rb^+, the Alk–NBO separations are 0.147 and 255 nm and the Alk–NBO–Si angles are 180° and 86°, respectively. It is this Alk–NBO–Si bending that causes 'rotation' of the O 2p orbital.

Overall, our simulations are consistent with Griscom's vision of a $\equiv$SiO· radical coupled to a nearby alkali cation [68]. It seems that this cation does not belong to a neighboring NBO (this distinction disappears if the cation is 'loosely' bound to this NBO) and its crystal field is not symmetric in the general case. The calculations suggest that

the observed NBO–Alk separation and the spin density on Alk^+ can be reproduced in a model where the cation does not leave the trapping site. Even without the stabilizing effect of the BOs, the NBO–Alk bond elongates rather than dissociates; when the cation interacts with several BOs this trend only increases. Such a picture naturally accounts for the formation of L-centers upon electron tunneling to OHC_1, which the model with a migrating cation leaves unexplained. Furthermore, low-amplitude swinging motion of the cation in a cage accounts for the observed asymmetric T_2 relaxation and temperature-dependent ESEEM spectra for OHC_1 in Na silicate glasses.

5.5. L-center

With this insight in the structure of OHC_1, one can make a better guess about the nature of the luminescence center. Trukhin et al. [32–38] suggested that the L-center is a triplet $\equiv$SiO··Alk species; Brekhovskikh and Tyul'kin [47] – that the excitation resides on SiO_4 units.

The MNDO calculation for the lowest triplet state of $(HO)_3SiOLi$ supports Trukhin's structure: In the optimum geometry, the NBO–Li bond is even more elongated than in the hole center (0.212 vs. 0.2 nm), the charge on Li and NBO are −0.2 and −0.24, respectively, while the spin density on these atoms is unity (as determined by Mulliken population analysis). However, the energy of this triplet state is too high, ca. 4.5 eV above the ground state as compared to the experimental 3.4 eV.

When the BOs were included, a different structure with much lower energy, ca. 3.7 eV above the ground state, was obtained. In this triplet center, the Li–NBO bond was still elongated, ca. 0.195 nm, but the charge on Li was +0.58 and the spin density on this atom was negligible. The Si′–NBO bond was elongated to 0.182 nm (from 0.16 nm) and the charges on NBO and Si′ atoms were −0.77 and +1.64, respectively (cf. −1.15 and +2.2 in the ground state). Mulliken population analysis gave the spin densities of 1.22 on NBO and 0.56 on Si′ atom. In terms of orbital structure, this center resembles the self-trapped triplet exciton in silica [93]. For example, similar MNDO calculation for the lowest triplet state of $Si(OH)_4$ yields a distorted tetrahedron in which a single Si–O bond is elongated to 0.19 nm with spin densities 1.16 and 0.7 and charges −0.43 and +1.63 on O and Si atoms, respectively.

We believe that the original model of the L-center proposed by Brekhovskikh and Tyul'kin is preferable to the biradical structure introduced by Trukhin et al. *The L-center is more correctly viewed as an exciton trapped on the Q_3 species than a $\equiv$SiO··Alk biradical.* The former structure naturally accounts for the formation of E′ and peroxy radicals in alkali silicate glasses (in full analogy to dissociation of triplet excitons in fused silica [93]) and is more consistent with the observed energetics. Since the alkali cation is strongly involved in this center, various data pointing to such an involvement (e.g., [36,37,51,52]) find their logical explanation. Actually, the Alk–NBO distance is *longer* in the biradical!

5.6. OHC_2

Modeling of OHC_2 is a challenging problem, and our simulations should be viewed with caution. Following Cases and Griscom [70] and Griscom [68], we first assumed that in this center the electron spin and negative charge are shared between two equivalent NBOs on the same SiO_4 tetrahedron. The simplest species of this type is a hole trapped on the $(HO)_2Si(O^-)_2$ (**VIII**).

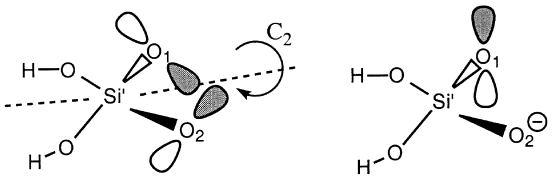

VIIIa **VIIIb**

There are two possibilities: (i) the spin is shared between the two equivalent NBOs (C_{2v} symmetry, **VIIIa**) and (ii) the spin is centered on one NBO and the charge on another (C_s or C_1 symmetry, **VIIIb**). Our MNDO and ab initio calculations indicate that the C_1 structure is 0.5–0.6 eV lower in energy than the C_{2v} structure. When the symmetry

is reduced from C_{2v} to C_s, the optimization procedure still converges to two *non-equivalent* NBOs. In **VIIIa**, r(Si–O) is 0.162 nm and the charge on NBO is −0.93. In **VIIIb**, the spin is centered on one NBO (charge −0.63, $r(\text{Si–O}_1) = 0.17$ nm) while the negative charge is mainly on the second NBO (charge −1.23, $r(\text{Si–O}_2) = 0.156$ nm).

This behavior can be accounted for by orbital symmetry analysis: The C_{2v} center **VIIIa** is a Jahn–Teller-active structure whose perturbation reduces the orbital energy. We have examined several larger models that included alkali cations and $(HO)_3$Si-terminated BOs, but the result was the same: equal sharing of spin and charge between the NBOs is energetically unfavorable. In fact, the involvement of alkali cations and side groups raises the barrier, since the Q_2 unit is more perturbed. The same result was obtained for holes trapped on Q_1 species.

Thus, *for the two NBOs be magnetically equivalent, the geometry of the trapping site must be different from that of a SiO_4 unit.* The only other possibility is to postulate a rapid exchange between two conformers of the asymmetrically distorted OHC_1-like center

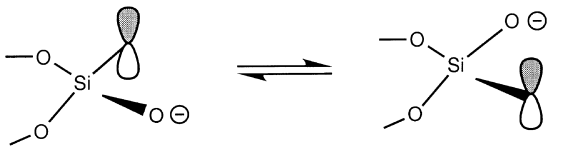

(10)

that causes dynamic averaging of magnetic parameters. We remind the reader that in an analogous spin center in pure silica, type-II self-trapped hole center (STH_2) [108], two BOs are magnetically equivalent due to *rapid tunneling* of the electron between two degenerate sites. Dynamic averaging for distorted tetrahedral $[GeO_4]^-$ and $[FeO_4]^-$ hole centers was observed in crystalline α-quartz (see, e.g., Refs. [109,110]).

It is easy to see that a thermally activated exchange (10) is inconsistent with EPR data. Such a reaction would require overcoming a barrier of ~0.5 eV; it would halt at cryogenic temperatures. The EPR spectrum from the OHC_2 does not change from 4 to 300 K. At elevated temperatures, the activated reaction (10) should be faster, making the g-tensor more symmetric. Instead, a reversible $OHC_2 \rightarrow OHC_1$ transformation was observed [68]. Thus, *the only viable mechanism is rapid tunneling between two degenerate sites.* How compatible is this mechanism with the data on spin relaxation and ESEEM in OHC_2?

The spin relaxation rate is given by $T_2^{-1} = 1/4\,\omega^2\tau_{ex}\langle\Delta\mathbf{g} : \Delta\mathbf{g}\rangle$, where $\Delta\mathbf{g} = \mathbf{g} - \langle\mathbf{g}\rangle$ and $\langle\,\rangle$ means averaging over the sites and τ_{ex} is the exchange time. Estimating $\langle\Delta\mathbf{g} : \Delta\mathbf{g}\rangle^{1/2}$ as $(0.5\text{–}1) \times 10^{-2}$ (the average $g_{xx} - g_{yy}$ for OHC_1) we find that to obtain observable T_2 of 0.3–1 μs at 4–180 K, the exchange time τ_{ex} should be 1-to-50 ps. This short time is reasonable for a tunneling reaction. The tunneling also explains low activation energy for T_p^{-1} ($\propto \tau_{ex}$) in the OHC_1, <10 meV. Furthermore, since $\omega\tau_c \ll 1$, $T_1 \approx T_2$ – in full agreement with the experiment.

^{23}Na ESEEM data further support the proposed structure for OHC_2 by indicating weaker coupling to Na^+ cation in this center relative to OHC_1. The transformation of OHC_2 to an OHC_1-like center at elevated temperatures can be explained by thermally activated migration of alkali cation and its binding to one of the NBOs. Coulombic interaction with the cation locks the hole center in one of conformations. This mechanism is similar to that proposed by Griscom [68].

The alternative of the dynamic averaging is a planar geometry for the OHC_2. Such a situation is possible when the hole is trapped on a $–SiO_2^-$ group (**IX**) yielding a neutral $–SiO_2^{\bullet}$ species. We modeled these hole centers using structures **X** and **XI**.

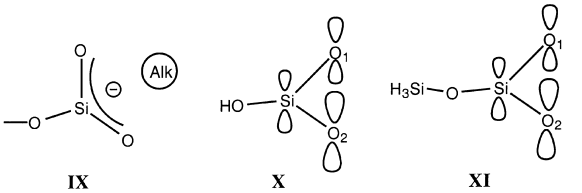

In **X**, the OH group either resides in the O–Si–O plane (C_s') or perpendicular to this plane (C_s''). In the C_s'' center, the charge on two equivalent NBOs is −0.68 and Si–NBO bond is 0.158 nm. The spin density is equally divided between two O 2p orbitals (0.72), but there is a considerable spin density on the Si 3p orbital (−0.4). In the C_s' center, the

charges on NBOs are −0.5 and −0.97, and the Si–NBO separations are 0.166 and 0.151 nm, respectively. The spin resides on the O 2p orbital of a more positively charged NBO; the spin density on the Si 3s orbital is close to that in **V**. The energy of the C_s'' conformer is 0.17 eV higher than that of the C_s' conformer: The equal sharing of negative charge between the NBOs is energetically favorable, as it results in lesser elongation of the Si–O bonds and smaller steric hindrance for the OH group.

Where would **X** absorb? Using molecular orbital energies, we estimated that **V** would absorb at 1.8 eV, the C_s' variant of **X** – at 1.66 eV and the C_s'' variant – at 0.8 eV. Although these estimates are crude, the absorption of the C_s' center is clearly red-shifted as compared to the C_s'' center. Same trends were observed for a larger structure **XI**, for which two geometries were considered, a symmetric (C_s) and asymmetric (C_1). Again, the broken-symmetry species had spin and absorbance parameters close to those of the ≡SiO· centers, while the symmetric species was ca. 0.1–0.15 eV lower in energy and absorbed at longer wavelengths.

These results suggest that a network-bound –SiO· radical is a reasonable candidate for OHC_2. This structure explains the symmetry of the *g*-tensor, equal sharing of spin between two NBOs, absorption properties, and conversion of OHC_2 to an OHC_1-like center at high temperature (through thermally activated asymmetric distortion). The planar structure accounts for the stability of the symmetric center towards Jahn–Teller distortion. Fast spin relaxation in the OHC_2 can be explained through low-amplitude tumbling of the $–SiO_2·$ rotor or rapid exchange between the conformers.

There is, however, a problem: In **X**, the spin density on the Si 3s orbital is 2–3 times higher than in **V**. Cases and Griscom [70,71] reported that in the OHC_2, the hfcc on ^{29}Si is ca. 1.5 mT which is comparable to 1.4 mT found for OHC_1 (K silicate glasses). Since it is likely that the symmetry is somewhat broken in the glass network (the energy gap between the symmetric and asymmetric states is narrow), the observed hyperfine structure is likely to be a result dynamic averaging between the conformers. Thus, the discrepancy between the expected and observed coupling constants on ^{29}Si does not mean that the proposed structure is incorrect.

The real challenge is explaining how the precursor of the OHC_2, the $–SiO_2^-$ Alk^+ defect, is formed. There are no analogous defect centers in crystalline silicates. It seems that the only way to produce this defect is via disproportionation of Q_n units. In contrast, tetrahedral center **VIII** has a readily identifiable precursor, a cation-stripped Q_2 species.

In conclusion, there are two possible ways to account for the observed EPR features of the OHC_2. One possibility is rapid tunneling reaction (6) between two degenerate sites of an OHC_1-like defect **VIIIb** with rate of $(0.2–10) \times 10^{11}$ s^{-1} over a barrier of ca. 0.5 eV. The second possibility is a planar $–SiO_2·$ unit. Further experimentation is needed to make the choice between these two models.

5.7. E' center

As was shown in Ref. [71], in this dangling bond center the spin density on Si is ~5% less than that in the E_γ' center fused silica. Cases and Griscom suggested that the reduction is by transfer of the spin density to a neighboring alkali cation. Calculations for $(HO)_3Si·Li^+$ and $(H_2SiO)_3Si·Li^+$ structures (with C_1, C_{3v}, or C_s symmetries) suggest that the lithium cation is strongly repulsed by the dangling bond and has no discernible effect on the spin density on silicon. Attachment of Li^+ to the NBO on a neighboring SiO_4 tetrahedron does not help either, since the structural distortions needed to keep Li^+ sufficiently close to the dangling bond is too costly energetically. However, when one of the BO is substituted with a NBO–Alk complex, as in the $(HO)_2(Li^+O^-)Si·$ radical, the reduction in the spin density occurs, by approximately the same factor as in the experiment. This is a subtle effect. In the optimized geometry, the O–Si–O angles and Si–O bonds do not change significantly, except for the Si–NBO bond which is ca. 3–5% longer than the Si–BO bond. In this species, the Si–Alk separation is ~0.3 nm. Assuming that the Si–NBO–Alk angle for K^+ and Na^+ is close to 108°, we estimate that the shortest Si–Alk separation would be

0.31–0.32 nm. Therefore, in agreement with the experiment, such a center should exhibit weak perturbation of the *g*-tensor by the crystal field of the cation. Our calculations suggest that the E′ center in alkali silicate glasses is a Si dangling bond on a pyramidal SiO_3 unit with one NBO.

5.8. Silicon peroxy radical

Since little is known about the extended structure of this radical, our simulations are exploratory. The peroxy radical in silica was modeled as a $(HO)_3Si–O'–O''\cdot$ radical. In the optimized geometry, the Si–O′–O″ angle is 120°, $r(Si–O') = 0.173$ nm and $r(O'–O'') = 0.12$ nm. The electrostatic charges and spin densities on O″ (O′) are −0.16 (−0.47) and 0.76 (0.25); the spin density is on the O 2p orbitals. These spin densities agree well with the data on ^{17}O satellite structure for Si peroxy radical in fused silica [111]. When Li^+ is added to the center, it binds to the O″ atom, with Li–O″ separation of 0.21 nm and Li–O″–O′ angle of 120°. In this complex, the charge and spin density on O″ increase to −0.26 and 0.38, respectively, and the charge and spin density on O′ decrease to −0.37 and 0.64, respectively; the Si–O′ bond elongates to 0.178 nm. These changes are smaller in the complex where Li^+ is coordinated to the BOs. For example, the spin densities on O″ and O′ are 0.7 and 0.3, respectively. We found that in all these complexes the spin density on Si was ca. −0.01 (of which -3×10^{-3} was on the Si 3s orbital), and did not significantly change when the cation was involved. This Si 3s density compares well with $(2–2.5) \times 10^{-3}$ found for peroxy radicals in silica [111] and alkali silicate glasses [71]. Thus, coupling of alkali cation to Si peroxy radical results in small changes in hfcc parameters. Since such a coupling is suggested by the ESEEM data, it is preferable to view the peroxy radical as a $\equiv SiOO\cdot Alk^+O^-Si\equiv$ complex.

It is instructive to compare the $(HO)_3SiO_2\cdot Li^+$ complex and the 'interstitial $O_2\cdot^-$ anion' modeled as the $\cdot O''–O'^-Li^+$ radical. A linear geometry with $r(O'–O'') = 0.12$ nm and $r(O'–Li) = 0.174$ nm was obtained for the latter; the spin densities on oxygens were 0.71 (O″) and 0.29 (O′). These densities are similar to those in alkali-coupled Si peroxy radicals. It is possible that these two radicals cannot be easily separated by EPR at 4–20 K, when their tumbling motion is arrested. At higher temperature, rapid dynamic averaging in the $O_2\cdot^-$ would make the oxygens magnetically equivalent and its *g*-tensor axially symmetric [71].

An intriguing question is, why only silicon peroxide radicals are present in irradiated silica while both such radicals and interstitial $O_2\cdot^-$ anions [71] occur in the alkali silicate glasses? This must be due to high basicity of the alkali silicates. Since only $O_2\cdot^-$ anions occur in the K silicate glasses above 580 K [71] these anions are more stable than the $\equiv SiOO\cdot$ radicals. Our ESE results indicate that only bonded radicals are present in the glass irradiated at 77 K. Therefore, we suggest that in basic glasses the peroxy radical is thermally unstable and yields $O_2\cdot^-$ upon the activation of the alkali cation migration (in analogy to reaction (11) in basic aqueous solution [112])

$$HO_2\cdot + HO^- \rightarrow O_2\cdot^- + H_2O \quad (pK_a \approx 4.5) \tag{11}$$

$$\equiv SiOO\cdot + \equiv SiO^-Alk^+ \rightarrow \equiv SiOSi\equiv + O_2\cdot^-Alk^+ \tag{12}$$

Using ab initio calculations we estimated that reaction (12) is exothermic by 0.07 eV (for OH-terminated species and Alk≡Li). Thermal activation is needed to dissociate the O^-Alk^+ bond. The efficiency of reaction (12) should increase with the optical basicity of the silicate glass. Interstitial O_2 is formed in recombination of superoxide anions with passing holes. Alternatively, it is the product of reactions initiated by the formation of a hole center in the vicinity of the peroxy/superoxide radical

$$\equiv SiO\cdot + \cdot OOSi\equiv \rightarrow \equiv SiOOOSi\equiv \text{ or } O_2 + \equiv SiOSi\equiv \tag{13}$$

$$\equiv SiO\cdot + Alk^+O_2\cdot^- \rightarrow \equiv SiO_3^-Alk^+ \tag{14}$$

$$\equiv SiOOOSi\equiv + \equiv SiO^-Alk^+ \rightarrow \equiv SiO_3^-Alk^+ + \equiv SiOSi\equiv \tag{15}$$

$$\equiv SiO_3^-Alk^+ \rightarrow \equiv SiO^-Alk^+ + O_2. \tag{16}$$

Reactions (13)–(16) are analogous to the formation/decay reactions of H_2O_3 and HO_3^- in basic water (see Section VI.E.4 in Ref. [112]).

6. Conclusion

Pulsed EPR and cw ENDOR of O- and Si-centered radicals in Li, Na, K and Cs silicate glasses was studied. The structure of these spin centers was simulated using semi-empirical and ab initio methods. Several structural and mechanistic insights were obtained.

For OHC_1, it was found that the Alk–NBO complex does not dissociate upon trapping the hole. The alkali cation remains coupled to the center and undergoes low-amplitude swinging motion inside the cage. This motion is activated at ~80 K in sodium and ~170 K in potassium glasses. It causes asymmetric T_2 relaxation and temperature-dependent ESEEM. A Q_3 unit is a likely precursor for the OHC_1. These hole centers are uniformly distributed in homogeneous alkali-loaded silicate glasses and selectively trapped in Na-rich islands in microscopically phase-separated alkali-deficient glasses. It appears that the OHC_1 in alkali silicates is not fully analogous to OHC centers in 'wet' silica.

For OHC_2, it is concluded that rapid T_1 and T_2 relaxation in this center is caused by rapid tunneling of electron between two degenerate OHC_1-like conformers. The alkali cation is not coupled to this center as strongly as in OHC_1. A likely precursor of this hole center is a $=SiO_2^{2-}$ unit. Alternatively, this center may be a hole on a planar $-SiO_2^-$ unit.

For E′ center, it is found that the alkali cation is not coupled to the dangling bond. This center is present in all silicate glasses. In phase-separated glasses, it is formed mainly in the Si-rich phase. Our work demonstrates that glass morphology may be studied by measurement of spin relaxation times of radiation-induced defects.

For peroxy/superoxide radicals, it is found that these species are neither hole nor electron centers; the radiolytic yield of these radicals is temperature-independent. It is speculated that the species are formed by dissociation of self-trapped excitons. L-centers are identified as such species, with spin density residing on a distorted Q_3 unit perturbed by the crystal field of the alkali cation. The peroxy/superoxide radicals are strongly coupled to the alkali modifier cations. We speculate that the superoxide anions are formed from the peroxy radicals via thermally activated reaction (12).

We found that the 'concentration vs. dose' dependences for hole centers were different from those of the silicon E′ and peroxy/superoxide radicals. For the hole centers, the growth of the concentration is much steeper, and saturates at $(1–5) \times 10^{18}$ cm^{-3}. For E′ and peroxy/superoxide radicals no saturation was observed up to 5 MGy. The similarity in dose dependences for E′ and peroxy/superoxide radicals suggests that these two centers are formed in the same radiolytic reaction.

No intrinsic spin-1/2 electron centers were found in cw EPR and pulsed EPR and ODMR spectra of alkali silicate glasses. Either the electrons are trapped by traces of metal impurity (Fe^{II}, Ti^{IV}) or the intrinsic electron centers are diamagnetic.

Acknowledgements

We are grateful to Dr D.L. Griscom for many helpful suggestions and insightful discussions. We thank Dr S. Michaeli for taking some cw EPR spectra. We gratefully acknowledge the help from Professor M. Makinen and Dr E. Galtseva (University of Chicago), Professor B.M. Hoffman (Northwestern University) and Dr J. Telser (Roosevelt University) with ENDOR experiments. This work was performed with financial support from the EMSP office of the US-DOE, grant No. 60416. The cost of equipment and facilities was supported by the BES office, Division of Chemical Science, US-DOE, under contract number W-31-109-ENG-38.

References

[1] I.A. Shkrob, B.M. Tadjikov, A.D. Trifunac, this issue, p. 1.
[2] W.J. Weber, R.C. Ewing, C.A. Angell, G.W. Arnold, A.N. Cormack, J.M. Delaye, D.L. Griscom, L.W. Hobbs, A. Navrotsky, D.L. Price, A.M. Stoneham, M.C. Weinberg, J. Mater. Res. 12 (1997) 1946.

[3] J.F. Natale, D.G. Howitt, Nucl. Instr. and Meth. B 1 (1984) 489, and references therein.
[4] D.G. Howitt, H.W. Chan, J.F. Natale, J.P. Heuer, J. Am. Ceram. Soc. 74 (1991) 1145.
[5] B.J. Todd, J.L. Lineweaver, J.T. Kerr, J. Appl. Phys. 31 (1960) 51.
[6] J.L. Lineweaver, J. Appl. Phys. 34 (1963) 1786.
[7] P.H. Dawson, Suppl. Nuovo Cim. 5 (1967) 612.
[8] S.A. Dikanov, Y.D. Tsvetkov, Electron Spin Echo Modulation (ESEEM) Spectroscopy, CRC, Ann Arbor, 1992.
[9] H. Kurreck, B. Kirste, W. Lubitz, Electron Nuclear Double Resonance Spectroscopy of Radicals in Solution, VCH, New York, 1988 (Chapters 1–4).
[10] G.N. Greaves, in: C.R. Catlow (Ed.), Defects and Disorder in Crystalline and Amorphous Solids, Kluwer Academic, Dordrecht, 1994, p. 87.
[11] G.N. Greaves, J. Non-Cryst. Solids 71 (1985) 203.
[12] D.A. McKeown, G.A. Waychunas, G.E. Brown Jr., J. Non-Cryst. Solids 74 (1985) 325.
[13] T.F. Soules, J. Chem. Phys. 71 (1979) 4570.
[14] S.K. Mitra, R.W. Hockney, Philos. Mag. B 48 (1983) 151.
[15] H. Inoue, I. Yasui, Phys. Chem. Glasses 28 (1987) 63.
[16] R.G. Newell, B.P. Feuston, S.H. Garofalini, J. Mater. Res. 4 (1989) 434.
[17] C. Huang, A.N. Cormack, J. Chem. Phys. 95 (1991) 3634.
[18] C. Huang, A.N. Cormack, J. Chem. Phys. 93 (1990) 8180.
[19] H. Melman, S.H. Garofalini, J. Non-Cryst. Solids 134 (1991) 107.
[20] W. Smith, G.N. Greaves, M.J. Gillan, J. Chem. Phys. 103 (1995) 3091.
[21] X. Yuan, A.N. Cormack, Mater. Res. Soc. Symp. Proc. 455 (1997) 242.
[22] C.M. Schramm, B.H.W.S. de Jong, V.E. Parziale, J. Am. Chem. Soc. 106 (1984) 4396.
[23] R. Dupree, D. Holland, P.W. McMillan, R.F. Pettifer, J. Non-Cryst. Solids 68 (1984) 399.
[24] J.F. Stebbins, J. Non-Cryst. Solids 106 (1988) 359.
[25] H. Maekawa, T. Maekawa, K. Kawamura, T. Yokokawa, J. Non-Cryst. Solids 127 (1991) 53.
[26] M.D. Ingram, Phys. Chem. Glasses 28 (1987) 215.
[27] P. Maass, J. Non-Cryst. Solids 255 (1999) 35.
[28] P. Maass, A. Bunde, M.D. Ingram, Phys. Rev. Lett. 68 (1992) 3064.
[29] S. Balasubramanian, K.J. Rao, J. Non-Cryst. Solids 181 (1995) 157.
[30] S. Balasubramanian, K.J. Rao, J. Phys. Chem. 97 (1993) 8835.
[31] D.R. Uhlmann, A.G. Kolbeck, Phys. Chem. Glasses 17 (1976) 146.
[32] A.N. Trukhin, Polish Ceram. Bull. 11 (1994) 7.
[33] A.N. Trukhin, J. Non-Cryst. Solids 123 (1990) 250.
[34] A.N. Trukhin, Phys. Stat. Solidi A 93 (1986) K185.
[35] A.N. Trukhin, M.N. Tolstoi, L.B. Glebov, V.L. Savelev, Phys. Stat. Solidi B 99 (1980) 155.
[36] A.N. Trukhin, L.B. Glebov, M.N. Tolstoi, Glass Phys. Chem. 14 (1989) 286.
[37] A.N. Trukhin, Z. Prikl. Spekt. 48 (1988) 138 (in Russian).
[38] A.N. Trukhin, L.E. Intenberg, V.L. Savel'ev, K.B. Glebov, M.N. Tolstoi, Sov. Phys. Solid State 27 (1985) 1862.
[39] A.N. Trukhin, Glass Phys. Chem. 8 (1983) 393.
[40] A.O. Volchek, A.I. Gusarov, A.P. Zhevlakov, D.O. Leshchenko, Opt. Spectrosc. 80 (1996) 390.
[41] S.S. Kurbanov, M.A. Kasymdzhanov, P.K. Khabibullaev, Dokl. Akad. Nauk 357 (1997) 180 (in Russian).
[42] M.A. Kasymdzhanov, S.S. Kurbanov, P.K. Khabibullaev, Glass Phys. Chem. 22 (1996) 464.
[43] M.A. Kasymdzhanov, S.S. Kurbanov, P.K. Khabibullaev, Busenges. Phys. Chem. 101 (1997) 1549.
[44] O.M. Efimov, K. Gabel, S.V. Garnov, L.B. Glebov, S. Grantham, M. Richardson, M.J. Soileau, J. Opt. Soc. Am. B 15 (1998) 193.
[45] J.H. Mackey, H.L. Smith, A. Halperin, J. Phys. Chem. Solids 27 (1966) 1759.
[46] C. Bettinali, P. Granati, Z. Phys. Chem. 70 (1970) 24.
[47] S.M. Brekhovskikh, V.A. Tyul'kin, Izv. Akad. Nauk. USSR: Inorg. Mater. 6 (1971) 1628 (English translation).
[48] G.H. Sigel Jr., J. Non-Cryst. Solids 13 (1973/74) 372.
[49] A.J. Cohen, G.G. Janezic, Phys. Stat. Solidi A 77 (1983) 619.
[50] L.N. Skuja, A.R. Silin, A.G. Boganov, J. Non-Cryst. Solids 63 (1984) 431.
[51] A.R. Kangro, M.N. Tolstoi, I.K. Vitol, Glass Phys. Chem. 4 (1978) 627.
[52] A.R. Kangro, M.N. Tolstoi, I.K. Vitol, J. Lumin. 20 (1979) 349.
[53] V.I. Arbuzov, I.K. Vitol Grabovskis, V.Ya. Grabovskis, M.N. Tolstoi, Glass Phys. Chem. 4 (1986) 400 (English translation).
[54] V.J. Grabovskis, J.J. Dzenis, N.S. Kovaleva, M.N. Tolstoi, Sov. Solid State Phys. 32 (1990) 2953.
[55] J.S. Stroud, J. Chem. Phys. 35 (1961) 844.
[56] J.W.H. Schreurs, R.F. Tucker, in: J.A. Prins (Ed.), Proceedings of the International Conference on the Physics of Non-Crystalline Solids, Delft, 1964, North-Holland, Amsterdam, 1964, p. 616.
[57] C.R. Kurkjian, G.E. Peterson, Phys. Chem. Glasses 15 (1974) 12.
[58] C.R. Kurkjian, G.E. Peterson, Solid State Comm. 11 (1972) 1105.
[59] S. Arafa, Phys. Chem. Glasses 15 (1974) 42, and references 1–7 therein.
[60] J.M. Baker, A.A. Jenkins, V.L. Savelev, W. Hayes, J. Phys. 2 (1990) 7453.
[61] D.L. Griscom, J. Non-Cryst. Solids 6 (1971) 275.
[62] D.J. DiMaria, in: S.T. Pantelides (Ed.), The Physics of SiO_2 and its Interfaces, Pergamon, New York, NY, 1978, p. 160.
[63] D.L. Griscom, J. Non-Cryst. Solids 40 (1980) 211.
[64] N. Itoh, Adv. Phys. 31 (1982) 491.
[65] A.E. Hughes, S.C. Jain, Adv. Phys. 28 (1979) 717.
[66] J.S. Stroud, Phys. Chem. Glasses 5 (1964) 71.
[67] J.S. Stroud, J. Chem. Phys. 37 (1962) 836.
[68] D.L. Griscom, J. Non-Cryst. Solids 31 (1978) 241.
[69] D.L. Griscom, J. Non-Cryst. Solids 64 (1984) 229.

[70] R. Cases, D.L. Griscom, in: Proceedings of the XVI International Congress on Glass, vol. 3; published in: Bol. Soc. Esp. Ceram. Vid. 31 C, 1992, p. 53.
[71] R. Cases, D.L. Griscom, Nucl. Instrum. and Meth. B 1 (1984) 503.
[72] D.L. Griscom, J. Non-Cryst. Solids 73 (1985) 51.
[73] M. Stapelbroek, D.L. Griscom, E.J. Friebele, G.H. Sigel Jr., J. Non-Cryst. Solids 32 (1979) 313.
[74] D.L. Griscom, in: B. Henderson, A.E. Hughes (Eds.), Defects and Their Structure in Nonmetallic Solids, Plenum, New York, 1976, p. 323.
[75] J.W.H. Schreurs, J. Chem. Phys. 47 (1967) 818.
[76] N.G. Cherenda, D.M. Yudin, Phys. Stat. Solidi B 67 (1975) 255.
[77] E.A. Zamotrinskaya, L.A. Torgashinova, V.F. Anufrienko, Izv. Akad. Nauk. 8 (1972) 1136 (English translation).
[78] J.H. Mackey, J.W. Boss, M. Kopp, Phys. Chem. Glasses 11 (1970) 205.
[79] T.A. Sidorov, V.A. Tul'kin, Dokl. Akad. Nauk SSSR 175 (1967) 872 (in Russian).
[80] G. Kordas, B. Camara, H.J. Oel, J. Non-Cryst. Solids 50 (1982) 79.
[81] G. Kordas, H.J. Oel, Phys. Chem. Glasses 23 (1982) 179.
[82] G. Kordas, Phys. Chem. Glasses 37 (1996) 9.
[83] L. Astrakas, Y. Deligiannakis, G. Mitrikas, G. Kordas, J. Chem. Phys. 109 (1998) 8612.
[84] L. Astrakas, G. Kordas, J. Chem. Phys. 110 (1999) 6871.
[85] L. Astrakas, G. Kordas, J. Non-Cryst. Solids 244 (1999) 205.
[86] H.A. El-Batal, N.A. Ghoneim, Glastech. Ber. Glass Sci. Techn. C 67 (1994) 215.
[87] F.M. Ezz-Eldin, I. Kashif, H.A. El-Batal, Radiat. Phys. Chem. 44 (1994) 39.
[88] O. Jbara, J. Cazaux, P. Trebbia, J. Appl. Phys. 78 (1995) 868.
[89] G. Battaglin, G. Della Mea, G. de Marchi, P. Mazzoldi, A. Miotello, Nucl. Instrum. and Meth. B 1 (1984) 511.
[90] R.G. Gossink, H. van Doveren, J.A.T. Verhoeven, J. Non-Cryst. Solids 37 (1980) 111.
[91] O. Gedeon, K. Jurek, V. Hulinsky, J. Non-Cryst. Solids 246 (1999) 1.
[92] A.I. MacGregor, R.K. MacCrone, J. Non-Cryst. Solids 102 (1988) 30.
[93] K.S. Song, R.T. Williams, Self-Trapped Excitons, Springer, Berlin, 1996, p. 270, and references therein (Chapter 7).
[94] R.L. Pfeffer, in: R.A.B. Devine (Ed.), The Physics and Technology of Amorphous SiO_2, Plenum, New York, 1987, p. 181.
[95] R.L. Pfeffer in: C.R. Helms, B.E. Deal (Eds.), The Physics and Chemistry of SiO_2 and the SiO_2–SiO_2 Interface, Plenum, New York, 1988, p. 169.
[96] T.E. Tsai, D.L. Griscom, Phys. Rev. Lett. 67 (1991) 2517.
[97] L. Zhang, V.A. Mashkov, R.G. Leisure, Phys. Rev. Lett. 74 (1995) 1605.
[98] L. Zhang, V.A. Mashkov, R.G. Leisure, Phys. Rev. B 53 (1996) 7182.
[99] L.B. Glebov, L.B. Popova, M.N. Tolstoy, V.V. Rusan, Fiz. Khim. Stekla 2 (1976) 569 (in Russian).
[100] N.G. Cherenda, A.V. Shendrik, D.M. Yudin, Phys. Stat. Solidi B 69 (1975) 687.
[101] Part III of this series, to be published.
[102] I.A. Shkrob, A.D. Trifunac, J. Phys. Chem. 107 (1997) 2374.
[103] I.A. Shkrob, D.W. Werst, A.D. Trifunac, J. Phys. Chem. 98 (1994) 13 262.
[104] D. Mao, P.C. Taylor, J. Non-Cryst. Solids 190 (1995) 48.
[105] S.A. Dzuba, H. Watari, Y. Shimoyama, A.G. Maryasov, Y. Kodera, A. Kawamori, J. Magn. Res. A 115 (1995) 80, and references therein.
[106] A.H. Edwards, J.A. Pickard, R.E. Stahlbush, J. Non-Cryst. Solids 179 (1994) 148.
[107] K.C. Snyder, W.B. Fowler, Phys. Rev. B 48 (1993) 13 238.
[108] D.L. Griscom, J. Non-Cryst. Solids 149 (1992) 137.
[109] M.J. Mombourquette, R.J. McEachern, J.A. Weil, Magn. Res. Chem. 33 (1995) S70.
[110] J. Minge, M.J. Mombourquette, J.A. Weil, Phys. Rev. B 40 (1989) 6523.
[111] D.L. Griscom, E.J. Friebele, Phys. Rev. B 24 (1981) 4896.
[112] Y. Tabata, Y. Ito, S. Tagawa, CRC Handbook of Radiation Chemistry, CRC, Boston, 1991, pp. 338 and 368.